

Research Articles | Development/Plasticity/Repair

Acoustic enrichment prevents early life stress-induced disruptions in sound azimuth processing

<https://doi.org/10.1523/JNEUROSCI.2287-24.2025>

Received: 3 December 2024

Revised: 19 February 2025

Accepted: 15 March 2025

Copyright © 2025 the authors

This Early Release article has been peer reviewed and accepted, but has not been through the composition and copyediting processes. The final version may differ slightly in style or formatting and will contain links to any extended data.

Alerts: Sign up at www.jneurosci.org/alerts to receive customized email alerts when the fully formatted version of this article is published.

1 Acoustic enrichment prevents early life stress-induced disruptions in sound
2 azimuth processing

3

4 Pengying An^{1,2,*}, Yue Fang^{1,2,*}, Yuan Cheng^{1,2}, Hui Liu^{1,2}, Wenjing Yang^{1,2}, Ye
5 Shan¹, Etienne de Villers-Sidani³, Guimin Zhang^{1,2,**}, Xiaoming Zhou^{1,2,**}

6

7 1, Key Laboratory of Brain Functional Genomics of Ministry of Education,
8 Shanghai Key Laboratory of Brain Functional Genomics, School of Life
9 Sciences, East China Normal University, Shanghai 200062, China

10

11 2, New York University-East China Normal University (NYU-ECNU) Institute of
12 Brain and Cognitive Science, NYU-Shanghai, Shanghai 200062, China

13

14 3, Department of Neurology and Neurosurgery, Montreal Neurological
15 Institute, McGill University, Montreal, QC H3A 2B4, Canada

16

17 *, These authors have contributed equally to this work

18

19 **, To whom correspondence may be addressed: G.Z.

20 (gmzhang@bio.ecnu.edu.cn) or X.Z. (xmzhou@bio.ecnu.edu.cn), Key
21 Laboratory of Brain Functional Genomics of Ministry of Education, East China
22 Normal University, Shanghai 200062, China

23

24 Abbreviated title: Acoustic enrichment prevents MS-induced deficits

25

26 Number of pages: 50

27 Number of figures: 9

28 Number of words for abstract: 195, introduction: 647, and discussion: 1500

29

30 **Acknowledgements:**

31 We thank Christoph Schreiner, Jufang He, and Robert Froemke for their
32 helpful discussions on earlier versions of this paper. X.Z. receives funding
33 from the National Science and Technology Innovation 2030 Major Program
34 (2022ZD0204804), the National Natural Science Foundation of China
35 (32161160325, 32171134, 32471059), the Joint Fund for Medicine and Health
36 from the ECNU (2022JKXYD08001), and the matching fund from the NYU-
37 ECNU Institute of Brain and Cognitive Science at the NYU Shanghai.

38

39 **Declaration of interests:**

40 The authors declare no competing interests.

41

42 **Abstract**

43 Early life stress (ELS) has been shown to disrupt cognitive and limbic
44 functions, yet its impact on sensory systems, particularly the auditory system,
45 remains insufficiently understood. In this study, we investigated the enduring
46 effects of ELS induced by neonatal maternal separation (MS) on behavioral
47 and cortical processing of sound azimuth in adult male rats. We found that MS
48 significantly impairs sound-azimuth discrimination, paralleled by broader
49 azimuth tuning and reduced dendritic branching and spine density in neurons
50 within the primary auditory cortex. Notably, exposure to an enriched acoustic
51 environment during the stress period effectively protects against these MS-
52 induced alterations, restoring behavioral performance, cortical tuning, and
53 dendritic spine density of neurons to levels comparable to controls. Further
54 analyses reveal that epigenetic regulation of cortical brain-derived
55 neurotrophic factor by histone H3 lysine 9 dimethylation may underlie the
56 observed changes in cortical structure and function. These results underscore
57 the profound and lasting impact of MS-induced ELS on auditory processing,
58 particularly within cortical circuits involved in spatial processing. They suggest
59 that sensory enrichment is a potential therapeutic strategy to ameliorate the
60 adverse effects of ELS on sensory processing, with broader implications for
61 understanding and treating sensory deficits in stress-related disorders.

62

63 **Keywords:** auditory cortex, behavioral discrimination, cortical processing,
64 early life stress, acoustic enrichment

65

66 **Significance Statement**

67 The contribution of early life stress (ELS) to sensory deficits in stress-
68 related disorders remains largely unexplored. Here we show that ELS induced
69 by neonatal maternal separation (MS) disrupts behavioral and cortical
70 processing of sound azimuth in adult rats. Moreover, pairing MS with enriched
71 acoustic exposure during the stress period alleviates these deficits in
72 maternally separated rats. Epigenetic modulation of brain-derived
73 neurotrophic factor gene expression by histone H3 lysine 9 dimethylation in
74 the cortex may underlie the MS-effects and their reversal through acoustic
75 enrichment. These findings reveal the enduring effects of ELS on sensory
76 processing, emphasizing its broader implications for understanding stress-
77 related disorders. Importantly, they highlight sensory enrichment as a
78 promising therapeutic strategy to prevent sensory deficits associated with
79 such conditions.

80

81 **Introduction**

82 Brain function depends on maintaining internal stability despite ever-
83 changing external environments, with stress responses representing a major
84 disruptor of this equilibrium. Previous studies in animal models have shown
85 that early life stress (ELS), such as that induced by neonatal maternal
86 separation (MS), often leads to lasting impairments in anxiety regulation,
87 learning and memory, and decision-making (Cao et al., 2014; Banqueri et al.,
88 2021; Alves et al., 2022; Kim et al., 2023). These functional disturbances are
89 accompanied by alterations in neurotransmitter levels, synaptic plasticity, and
90 neuronal morphology (e.g., dendritic branching and spine density) within
91 critical brain regions including the prefrontal cortex (Monroy et al., 2010;
92 Muhammad et al., 2012; Chocyk et al., 2013; Farrell et al., 2016),
93 hippocampus (Monroy et al., 2010; Cao et al., 2014; Ohta et al., 2017; Kim et
94 al., 2023), amygdala (Manzano-Nieves et al., 2020), and nucleus accumbens
95 (Monroy et al., 2010; Muhammad et al., 2012). These findings underscore the
96 profound impact of MS-induced ELS on the development of cognitive and
97 emotional functions.

98 The sensory systems of the mammalian brain are known to develop and
99 mature earlier than its cognitive functions, making them particularly
100 susceptible to environmental influences during early development. For
101 example, rodent studies have shown that while cognitive systems continue to
102 refine throughout the juvenile and adolescent periods (Alberini and Travaglia,
103 2017), the auditory system, including auditory pathways and cortical areas,
104 undergoes rapid maturation during the early postnatal period (de Villers-Sidani
105 et al., 2007; Insanally et al., 2009; Barkat et al., 2011; Nakamura et al., 2020).

106 During this critical developmental window, environmental stimuli and
107 experiences exert significant and enduring effects on auditory processing and
108 integration (Zhang et al., 2001; Han et al., 2007; Zhou and Merzenich, 2008;
109 Polley et al., 2013; Suta et al., 2015; Bures et al., 2017,2021; Pysanenko et
110 al., 2018; Svobodova Burianova and Syka, 2020; Tang et al., 2022). In
111 addition, sensory systems are interconnected with other brain structures
112 essential for cognitive functions via direct and indirect pathways, thereby
113 contributing to various higher cognitive functions (Moxon et al., 1999;
114 Mohedano-Moriano et al., 2007; Kraus and Canlon, 2012; Xiao et al., 2018;
115 Zhao et al., 2018). The differential timing in the maturation of sensory and
116 cognitive systems suggests that early sensory inputs can profoundly influence
117 cognitive development, particularly if sensory functions are disrupted during
118 the critical periods.

119 However, few studies to date have investigated the long-term effects of
120 MS-induced ELS on sensory processing. In the auditory system, Ye et al.
121 (2023) recently showed that ELS induced by a combination of MS and
122 restraint disrupts both the behavioral detection and neural encoding of rapid
123 sound signals in adult gerbils. Despite these significant results, the precise
124 neural mechanisms through which ELS affects auditory function later in life
125 remain largely unknown.

126 Sound localization is a fundamental task of the auditory system, with the
127 auditory cortex playing a key role in spatial sound processing (Jenkins and
128 Merzenich, 1984; Kavanagh and Kelly, 1987; Heffner and Heffner, 1990;
129 Zhang et al., 2013; Cheng et al., 2017,2020). It enables efficient navigation,
130 communication, and interaction with the environment by providing critical

131 spatial auditory information. In humans, spatial hearing helps distinguish
132 between different speakers, facilitating speech comprehension in social
133 settings and noisy places, e.g., where multiple conversations occur
134 simultaneously (Hawley et al., 2004; Grothe et al., 2010; Zündorf et al., 2013).
135 However, the specific effects of MS-induced ELS on the auditory cortex and
136 its implications for sound localization have not been thoroughly investigated.

137 In this study, we examined physiological changes within the primary
138 auditory cortex (A1) and their impact on spatial behavior in adult rats following
139 neonatal MS. We also explored structural and molecular changes in the cortex
140 and their epigenetic modifications to understand the enduring effects of MS on
141 adult rats. Finally, we assessed whether enriched sound exposure during MS
142 could protect against the observed alterations in behavioral and cortical
143 processing of sound azimuth in maternally separated rats.

144

145 **Materials and Methods**

146 Pregnant Sprague-Dawley (SD) rats were purchased from Shanghai
147 Slack Laboratory Animal Co., Ltd. (China) and housed individually in cages
148 (41×26×20 cm) at the Animal Experiment Center of East China Normal
149 University. Housing conditions were kept at 21±1 °C with 45-55% humidity
150 and an automatic 12/12-h light-dark cycle. The animals had ad libitum access
151 to food and water. All experimental procedures were approved by the
152 Institutional Animal Care and Use Committee of East China Normal
153 University. Every effort was made to minimize animal suffering and reduce the
154 number of animals used.

155 **Neonatal MS**

156 Male offspring from timed-pregnant SD rats were cross-fostered to form
157 litters of 10 per each at postnatal day (PND) 1 (birth was designated as
158 PND0). The pups were then randomly assigned to either MS or control group,
159 with 5 pups per group. The MS protocol was based on early studies with
160 minor modifications (Shin et al., 2019; Talani et al., 2023). Briefly, five pups
161 were gently placed into a clean cage, transferred to a different room, and kept
162 in a temperature-controlled incubator (26 ± 2 °C, 45-55% humidity) for 3 h daily
163 (10:00 to 13:00) from PND2 to 20. After the 3-h separation, the pups were
164 returned to their home cage with their dams. Control pups were handled twice
165 daily at 10:00 and 13:00, being moved from one side of the cage to the other,
166 but remained with their dams throughout.

167 At weaning (PND21), all pups were separated from their dams and
168 housed in groups of four per cage until PND56, during which various
169 experimental procedures were conducted.

170 **Enriched sound exposure**

171 The MS pups were exposed to an enriched acoustic environment (EAE)
172 during their daily 3-h MS period in the incubator from PND2 to 20. Acoustic
173 stimuli consisted of pulse trains with a duration of 1 s, containing 2, 5, 10, or
174 15 tone pips (50 ms duration with 5 ms ramps). The frequency of each tone
175 pip in the pulse train was set at 1.5, 2.3, 3.5, 5.3, 8.1, 12.3, 19, or 29 kHz.
176 These pulse trains with different frequencies and repetition rates were
177 randomly delivered at ~65 dB sound pressure level (SPL) as measured at the
178 center of the incubator. To minimize adaptation, a silent interval (randomly set

179 at either 0.5 or 1 s) was introduced between pulse trains. After weaning at
180 PND21, pups were housed in groups of four per cage until PND56 for
181 experiments.

182 **Open field test**

183 The open field test was conducted in a rectangular box (42×42×37 cm).
184 During the test, each rat was placed in the center of the box, facing the wall,
185 and allowed to explore freely for 15 min. The total distance traveled was
186 recorded and analyzed using the True-Scan System (Coulbourn Instruments,
187 USA). The box was cleaned with 75% ethanol between tests.

188 **Elevated zero-maze test**

189 The elevated zero-maze consisted of a circular platform (5.5 cm wide)
190 with an outer diameter of 92 cm, featuring two open arms and two closed
191 arms positioned opposite each other. The closed arms had 20 cm high walls,
192 while the open arms had no barriers. The apparatus was raised 50 cm above
193 the floor. During testing, each rat was placed in one of the open arms, facing a
194 closed arm, and allowed to explore freely for 5 min. Behavior was recorded
195 and analyzed using the ANY-maze system (Stoelting, USA). Between tests,
196 the maze was cleaned with 75% ethanol.

197 **Sound-azimuth discrimination task**

198 A wooden semicircular apparatus with a 150 cm radius was used for the
199 sound-azimuth discrimination task. At the center, a starting box (20×7×8 cm)
200 allowed the rats to initiate the task by running forward. Speakers were
201 positioned at 10° intervals along the curved wall, each with a waterspout
202 beneath. Water from these spouts was delivered via an automatic lick-

203 detection system. Each trial consisted of six bursts of white noise (50 ms
204 duration, 5 ms rise-decay, ~65 dB SPL) randomly emitted at 2 pulses per
205 second (pps) from one of the speakers. Rats were trained to identify the
206 sound azimuth and lick the corresponding waterspout for a water reward.

207 Rats had ad libitum access to food but were water-restricted prior to the
208 task (Rutkowski and Weinberger, 2005; Zhang et al., 2013; Cheng et al.,
209 2020). The task was conducted in a soundproof, double-walled room. The
210 behavioral task consisted of two phases: pre-training and training. In the five-
211 day pre-training phase, rats learned to exit the starting box, approach a
212 waterspout, and lick it to receive water in response to auditory cues from a
213 fixed angle (0°). In the training phase, rats were placed in the starting box
214 facing forward. They left the starting box after random sound bursts were
215 played from one of the speakers. The trial concluded when rats licked a spout.
216 If they approached and licked the spout under the correct speaker, they
217 received 2-3 drops of water as a reward, marking the trial as successful. If
218 they licked an incorrect spout, the trial was recorded as an error. The rats
219 returned to the starting box after each trial.

220 Each rat participated in ~35 trials per day, with the percentage of correct
221 responses calculated at the end of each day. The task was considered
222 complete once a rat achieved ≥70% correct responses on 2 of 3 consecutive
223 training days.

224 **Auditory brainstem response (ABR) and cortical recording**

225 Recordings were conducted in a soundproof, double-walled room. As
226 described previously (Zhang et al., 2013; Liu et al., 2019; Cheng et al.,

227 2020,2023), rats were anesthetized with an intraperitoneal injection of sodium
228 pentobarbital (50 mg per kg body weight). Areflexia was maintained with
229 supplemental doses of 8 mg/ml dilute pentobarbital during surgery and
230 recording sessions. Body temperature was continuously monitored using a
231 rectal probe and maintained at ~37 °C with a feedback-controlled heating pad.

232 ABRs were recorded using three subdermal electrodes placed at the
233 scalp midline, posterior to the stimulated ear, and on the midline of the back 1-
234 2 cm posterior to the neck. Tone pips (3, 10, 15, or 20 kHz) at different
235 intensities were generated using TDT System III (Tucker-Davis Technologies,
236 USA) and delivered through a calibrated earphone with a sound tube inserted
237 into the external auditory meatus. ABR signals were acquired, filtered,
238 amplified, and analyzed using equipments and software manufactured by
239 Tucker-Davis Technologies (USA). The ABR threshold was defined as the
240 lowest sound intensity capable of eliciting a characteristic response pattern.

241 For cortical recording, a 2 cm flat-headed nail was adhered to the
242 exposed skull with acrylic glue and dental cement. The rat's head was
243 secured in a head-holder, with the eye-snout line aligned to 0° azimuth and 0°
244 elevation in the frontal auditory field. After reflecting the temporalis muscle,
245 the auditory cortex was exposed, and the dura was carefully removed.
246 Parylene-coated tungsten microelectrodes (1-2 MΩ at 1 kHz; FHC, USA),
247 which were inserted perpendicularly into the cortex at a depth of ~450-550 μm
248 (layer IV; Games and Winer, 1988; Roger and Arnault, 1989), were used to
249 record the spike activity of individual neurons or small neuron clusters. The A1
250 location was identified according to the Paxinos and Watson atlas (Paxinos
251 and Watson, 2005) and other studies (Polley et al., 2006,2007; Rutkowski et

252 al., 2003). Neurons in A1 typically exhibit short-latency responses to tone pips
253 at specific frequencies.

254 Acoustic stimuli (tone pips of 50 ms duration, 5 ms rise-decay) were
255 played from a speaker placed 34 cm away from the rat's head. The speaker
256 was moved to different azimuths in the frontal auditory space using a remote-
257 controlled system operated by electric motors. Recordings began with stimuli
258 emitted from a speaker positioned 30° contralateral to the recording site
259 (c30°). The cortical responses evoked were recorded and frequency tuning
260 curves were constructed by presenting pure tones at 50 different frequencies
261 (1-30 kHz) across eight sound intensities (ranging from 0 to 70 dB SPL in 10-
262 dB steps) in a randomized, interleaved manner at a rate of 2 pps.

263 Characteristic frequencies (CFs) were defined for neurons at each cortical site
264 as the frequency that elicited a reliable response at the lowest threshold (i.e.,
265 minimum threshold, MT). After determining the CF and MT at each recording
266 site, the number of responses elicited by CF stimuli (20 dB above the MT) was
267 recorded at 10° intervals, from 90° contralateral (c90°) to 90° ipsilateral (i90°)
268 relative to the recording site. These stimuli were presented 32 times at each
269 azimuth, and the azimuth-selectivity curve was plotted by correlating the total
270 spike count (adjusted for spontaneous activity) with the azimuth angle.

271 Software programs (SigCal, SigGen, and Brainware; Tucker-Davis
272 Technology, USA) were used for speaker calibration, stimulus generation,
273 online monitoring of cortical responses, and data storage for later analysis.

274 Azimuth-selectivity curves were classified into four categories based on
275 their shapes: azimuth-selective, hemifield, multipeak, or nonselective.

276 Azimuth-selective curves featured a prominent peak at a specific angle that is

277 at least 50% higher than the minimum at both lateral angles. Hemifield curves
278 started at an ipsilateral angle, increased by more than 50%, and then either
279 plateaued or decreased by less than 50% across a broad range of
280 contralateral angles. Multiplex curves displayed two distinct peaks, each
281 exceeding the trough and lateral angles by at least 50%. Lastly, nonselective
282 curves lacked a clear peak, with spike counts across all angles varying by less
283 than 50%.

284 **Corticosterone analysis**

285 Rats were anesthetized with pentobarbital (50 mg/kg body weight), and
286 blood samples were collected and stored at 4 °C overnight to allow clotting.
287 The following day, the samples were centrifuged at 3000 rpm for 10 min to
288 separate the serum. Serum corticosterone levels were measured using an
289 enzyme-linked immunosorbent assay (ELISA) kit (Shanghai Xinyu
290 Biotechnology, China) following the manufacturer's instructions.

291 **Morphological analysis of neurons**

292 Four-week-old rats were anesthetized with pentobarbital (50 mg/kg body
293 weight) and secured in a stereotaxic apparatus (Stoelting, USA). After
294 exposing the skull, small holes were drilled above both hemispheres of the
295 auditory cortex. A total volume of 200 nl of recombinant adeno-associated
296 virus (AAV-sparse-NCSP-YFP-2E5; Braincase, China) was bilaterally injected
297 into the A1 at coordinates (AP: -4.5 mm, ML: \pm 6.5 mm, DV: -4.5 mm; Paxinos
298 and Watson, 2005) using a syringe. The virus was delivered at 20 nl/min using
299 a micro-infusion pump (RWD, China). After injection, the needle remained in
300 place for 10 min to allow diffusion, and the scalp was sutured. The animals

301 were returned to their home cages for recovery after waking from anesthesia.
302 A four-week recovery period ensured full healing and optimal viral expression.

303 After the four-week recovery, rats were deeply anesthetized with
304 pentobarbital (80 mg/kg body weight) and perfused intracardially with saline
305 followed by 4% paraformaldehyde in 0.1 M potassium phosphate-buffered
306 saline (pH 7.2). The brains were extracted and immersed in the same fixative
307 with 20% sucrose for 12-24 h. Brain tissue was sectioned coronally at a
308 thickness of 100 μ m using a freezing microtome (Leica CM3050S, Germany).
309 Sections were rinsed with phosphate-buffered saline (PBS) and mounted onto
310 slides. Images of layer IV pyramidal neurons in A1 were captured using
311 single-photon confocal microscopy (Leica SP8, Germany).

312 For spine density analysis, the acquired images were processed in Fiji
313 software (NIH, USA), and dendritic spines were traced and categorized into
314 stubby, mushroom, or thin subtypes (Yang et al., 2014; Tang et al., 2022).
315 Stubby spines were defined as having a large head closely attached to the
316 dendritic shaft without a distinct neck, mushroom spines had a large head and
317 narrow neck, and thin spines had a small head and elongated thin neck.
318 Spine density was calculated as the average number of spines per 10 μ m
319 segment of tertiary apical or basal dendrites.

320 In addition, dendrites were traced and cortical neuron morphology was
321 reconstructed using the NeuronJ plug-in in Fiji. Sholl analysis quantified
322 dendritic complexity by counting intersections of dendrites with concentric
323 circles, incrementally spaced 10 μ m apart from the soma.

324 **Western blotting**

325 Rats were deeply anesthetized with pentobarbital (80 mg/kg body weight).
326 Following decapitation, the brains were quickly removed, and the A1 (Paxinos
327 and Watson, 2005) were dissected. The tissue was homogenized in RIPA
328 buffer (50 mmol/L Tris pH 7.5, 150 mmol/L NaCl, 1% Triton X-100, 0.1% SDS,
329 2 mmol/L EDTA, 0.5% sodium deoxycholate) containing protease inhibitor
330 cocktail, as previously described (Liu et al., 2019; Tang et al., 2022). Equal
331 amounts of protein from each sample were separated by 10% sodium dodecyl
332 sulfate-polyacrylamide gel electrophoresis (SDS-PAGE) and transferred to
333 polyvinylidene fluoride (PVDF) membranes (Millipore, USA). The membranes
334 were blocked with 5% non-fat dry milk in Tris-buffered saline (TBS) (150 mM
335 NaCl, 20 mM Tris-HCl, pH 7.4) for 1.5 h at room temperature (RT), followed
336 by overnight incubation at 4 °C with primary antibodies. After three washes
337 with TBST (containing 0.1% Tween 20 in TBS), the membranes were
338 incubated with horseradish peroxidase (HRP)-conjugated secondary
339 antibodies for 1 h at RT. Following additional washes, protein bands were
340 visualized using the ChemiDoc™ XRS+ System (Bio-Rad, USA), and the
341 grayscale values of the bands were quantified using ImageJ software (NIH,
342 USA). The primary antibodies used in this study were: rabbit anti-H3K9me2
343 (1:1000; Cell Signaling Technology, USA), rabbit anti-BDNF (1:800;
344 Proteintech, USA), and rabbit anti- β -actin (1:1000; Proteintech, USA).

345 **Experimental design and statistical analysis**

346 Body weight, locomotor activity, anxiety-related behavior, and serum
347 corticosterone levels were assessed as described above and compared
348 across rat groups to confirm the induction of ELS by MS. In addition, ABR
349 parameters, cortical tuning, dendritic spine density, and molecular expression

350 were analyzed to investigate the effects of MS-induced ELS on sound azimuth
351 processing. Finally, the combination of MS and enriched acoustic exposure
352 was explored to evaluate its potential to protect against alterations in sound
353 azimuth processing in maternally separated rats.

354 Statistical comparisons were conducted using either an unpaired
355 Student's t-test, Mann-Whitney test, or one- or two-way Analysis of Variance
356 (ANOVA), depending on the experimental design. Prior to analysis, the
357 Kolmogorov-Smirnov test was used to evaluate the normality of the data
358 distribution. If significant effects were detected in the ANOVA, post hoc tests
359 were performed for multiple comparisons. In addition, cumulative data
360 distributions were compared across groups using the Kolmogorov-Smirnov
361 test and proportion data were analyzed using the χ^2 test. Differences were
362 considered statistically significant at $p < 0.05$.

363

364 **Results**

365 **Fig. 1** outlines the experimental timelines and procedures for the study.
366 To confirm that ELS was induced by MS, we assessed several stress
367 indicators, including body weight, locomotor activity, anxiety-related behavior,
368 and serum corticosterone levels, in MS rats and age-matched controls at
369 specific PNDs. On PND56, the animals were subjected to a sound-azimuth
370 discrimination task, ABR recordings, cortical recordings, dendritic spine
371 assessment, and molecular expression analysis to evaluate the lasting effects
372 of MS on young adult rats.

373 **Signs of ELS following MS**

374 The body weights of both MS and control groups on different PNDs are
375 presented in **Fig. 2A** and **B**. Statistical analysis revealed that the MS group
376 had a consistently lower body weight than the control group (two-way ANOVA,
377 $F(1,483)=28.00$, $p<0.001$; post hoc Student-Newman-Keuls test $p<0.001$ -
378 0.007 on PND35, 42, 49, and 56 but $p>0.31$ at other time points). Thus, early
379 MS resulted in a moderate, lasting reduction in body weight, persisting at least
380 until PND56.

381 Next, we conducted an open field test on PND21 and 56 to investigate the
382 potential impact of MS on locomotor activity (**Fig. 2C**). As shown in **Fig. 2D**,
383 the distance traveled by MS group during the different test periods was
384 comparable to that by control group on both PND21 and 56 (two-way ANOVA,
385 $F(1,111)=2.81$, $p=0.10$ on PND21 and $F(1,150)=0.02$, $p=0.89$ on PND56).
386 These data suggest that MS has little effect on locomotor activity in the rats.

387 We also evaluated anxiety-related behaviors using the elevated-zero
388 maze test (**Fig. 2E**). As shown in **Fig. 2F**, the total distance traveled by the
389 MS group was similar to that traveled by the control group on PND21
390 (unpaired Student's t-test, $t(34)=0.67$, $p=0.51$). However, the MS group
391 exhibited lower open arm entries (unpaired Student's t-test, $t(34)=2.45$,
392 $p=0.02$) and spent significantly less time in the open arms (unpaired Student's
393 t-test, $t(34)=2.08$, $p=0.045$), indicating increased anxiety-like behavior. On
394 PND56, although the MS group traveled a shorter total distance compared to
395 the control group (unpaired Student's t-test, $t(24)=2.58$, $p=0.017$), no
396 significant differences between the groups were observed regarding open arm
397 entries (unpaired Student's t-test, $t(24)=1.10$, $p=0.28$) or time spent in the
398 open arms (Mann-Whitney test, $p=0.57$). Therefore, early MS led to increased

399 anxiety-related behaviors during the juvenile period, but these behaviors
400 appeared to normalize by adulthood.

401 To further assess stress levels in rats following MS, we measured serum
402 corticosterone levels on PND21 and 56 (**Fig. 2G**). On PND21, the MS group
403 had significantly higher corticosterone levels compared to the control group
404 (Mann-Whitney test, $p < 0.0001$), but no significant differences were found on
405 PND56 (unpaired Student's t-test, $t(30) = 1.56$, $p = 0.13$). These results indicate
406 an acute corticosterone response to MS that diminishes by adulthood.

407 **Performance in the sound-azimuth discrimination task**

408 To determine the effects of early MS on behavioral processing of sound
409 azimuth in adulthood, we compared the performance of MS and control rats in
410 a sound-azimuth discrimination task on PND56. In this task, rats were trained
411 to localize the azimuth of a sound stimulus and then lick the associated water-
412 spout for a reward (see also **Materials and Methods**). As shown in **Fig. 3A**,
413 the percentage of correct trials increased gradually for both MS and control
414 rats as training progressed (two-way ANOVA, $F(16,218) = 37.02$, $p < 0.001$),
415 indicating that both groups learned to identify and selectively respond to a
416 new, randomly set target location. However, the average correct responses by
417 the MS group were lower than those by the control group throughout the
418 training period (two-way ANOVA, $F(1,218) = 156.79$; post hoc Student-
419 Newman-Keuls test $p < 0.001$ - 0.023 on training days 2-15 but $p > 0.17$ on other
420 days). Specifically, the MS group took an average of 9.3 ± 1.0 d and 17.6 ± 0.9 d
421 to achieve 50% and 70% accuracy, respectively, which was significantly
422 longer than the respective 5.4 ± 0.5 d and 9.8 ± 0.8 d taken by the control group

423 (**Fig. 3B**; unpaired Student's t-test, $t(15)=3.46$, $p=0.003$ for 50% cut-off and
424 $t(15)=6.38$, $p<0.001$ for 70% cut-off).

425 We also calculated the azimuth deviation (AD) as an index of
426 performance in the error trials. AD represents the angular difference between
427 the spout the rat licked and the position of the target speaker. Positive or
428 negative AD values indicate that the spout was to the right or left of the target
429 speaker, respectively. As shown in **Fig. 3C**, the proportions of positive and
430 negative ADs were comparable on each training day (two-way ANOVA,
431 $F(1,264)=1.92$, $p=0.17$ for the MS group and $F(1,200)=2.83$, $p=0.094$ for the
432 control group), indicating no azimuth preference for either group during the
433 task. Furthermore, we compared the absolute AD values between the MS and
434 control groups, with smaller ADs indicating higher performance accuracy. As
435 shown in **Fig. 3D**, AD values decreased with training for both groups (two-way
436 ANOVA, $F(16,218)=15.79$, $p<0.001$), but the average values for the MS group
437 consistently remained larger than those for the control group throughout the
438 training period (two-way ANOVA, $F(1,218)=47.22$, $p<0.001$; post hoc Student-
439 Newman-Keuls test $p<0.001-0.044$ for training days 1,4-6,9,10,13 but $p>0.05$
440 on other days).

441 Taken together, these data show that the task performance of the MS
442 group was consistently poorer than that of the control group when tested in
443 adulthood, indicating that MS-induced ELS impairs sound-azimuth
444 discrimination.

445 **Thresholds and wave latencies of ABRs**

446 To ensure that the lower performance of MS rats in the sound-azimuth
447 discrimination task was not simply due to alterations in hearing sensitivity
448 resulting from MS, we recorded the ABRs and compared the ABR
449 parameters, including thresholds and wave latencies, between MS and control
450 groups on PND56 (**Fig. 4A and B**). As shown in **Fig. 4C**, the ABR thresholds
451 for the MS group were comparable to those for the control group at various
452 frequencies (two-way ANOVA, $F(1,68)=0.022$, $p=0.88$). Furthermore, there
453 were no significant differences in the ABR latencies of waves I and IV
454 between the two groups (**Fig. 4D**; two-way ANOVA, $F(1,68)=0.37$, $p=0.55$ for
455 wave I and $F(1,68)=0.43$, $p=0.51$ for wave IV). These findings suggest that
456 neonatal MS has little impact on hearing thresholds and neural conduction
457 velocities within the brainstem.

458 **Sound azimuth selectivity of neurons in cortical field A1**

459 The response selectivity and reliability of cortical neurons contribute to the
460 accuracy of auditory-related behaviors (Zhang et al., 2013; Cheng et al.,
461 2017,2020; Francis et al., 2018; Liu et al., 2019; Tang et al., 2022). To
462 investigate the neural basis for behavioral changes induced by MS, we
463 documented azimuth tuning of cortical neuron by constructing azimuth
464 selectivity curves on PND56 and compared the findings for the MS and control
465 rats (**Fig. 5A and B**).

466 As detailed in **Materials and Methods**, all recorded azimuth selectivity
467 curves were categorized as being either azimuth-selective, multipeak,
468 hemifield, or nonselective (**Fig. 5B**). The distribution analysis revealed that the
469 MS group exhibited significantly lower percentages of azimuth-selective and

470 hemifield neurons but a higher percentage of multipeak neurons compared to
471 the control group (**Fig. 5C**; χ^2 test, $p < 0.001$ for azimuth-selective, $p = 0.005$ for
472 hemifield, and $p < 0.001$ for multipeak). The percentages of nonselective
473 neurons were similar for the two groups (χ^2 test, $p = 0.057$).

474 We next quantified two indices for each recorded azimuth-selective curve:
475 the angular range (AR), defined as the width at half maximum of the curve,
476 and the slope, calculated as half the sum of the slopes for both limbs of the
477 curve. The slope for each limb was determined by dividing the change in
478 normalized response (10% to 90%) by the corresponding azimuth range over
479 which this change occurred. The AR and the slope were used as measures of
480 selectivity and sensitivity, respectively, of cortical neurons to sound azimuth
481 variations; a smaller AR and higher slope of an azimuth-selective curve
482 indicate sharper tuning and higher sensitivity. Our data showed a significant
483 rightward shift in the AR distribution (i.e., larger ARs) for the MS compared to
484 control groups (**Fig. 5D**; Kolmogorov-Smirnov test, $p < 0.0001$). Further
485 analysis confirmed that the MS group had larger average AR compared to the
486 control group (**Fig. 5E**; Mann-Whitney test, $p = 0.008$). In contrast, the slope
487 distribution of azimuth-selective curves showed a significant leftward shift (i.e.,
488 lower slopes) for the MS compared to control groups (**Fig. 5F**; Kolmogorov-
489 Smirnov test, $p = 0.001$). Consistent with this, the average slope for the MS
490 group was significantly lower than that for the control group (**Fig. 5G**; unpaired
491 Student's t-test, $t(15) = 3.21$, $p = 0.006$). Additionally, the intensity thresholds for
492 these neurons were significantly higher in the MS group compared to the
493 controls (24.3 ± 0.8 vs. 21.0 ± 0.8 dB SPL; Mann-Whitney test, $p < 0.001$), and

494 their response latencies were notably longer (12.8 ± 0.3 vs. 11.4 ± 0.2 ms;
495 Mann-Whitney test, $p < 0.001$).

496 Collectively, these results suggest that MS significantly degrades the
497 sound azimuth tuning of cortical neurons in adult rats.

498 **Dendritic arborization and spine density of cortical neurons**

499 As described in **Materials and Methods**, above electrophysiological data
500 were primarily obtained from neurons in the granular layer (layer IV) of A1. To
501 investigate the structural basis of altered cortical spatial processing after MS,
502 we compared the dendritic arborization and spine density of pyramidal
503 neurons in this cortical layer between MS and control groups on PND56.

504 The effects of MS on dendritic arborization of cortical neurons were
505 assessed using Sholl concentric ring analysis. As illustrated in **Fig. 6A** and **B**,
506 there were significantly fewer intersections between dendritic branches and
507 Sholl circles in the proximal segments (40-80 μm from the soma) in the MS
508 compared to the control groups (two-way ANOVA, $F(1,826)=4.62$, $p=0.032$;
509 post hoc Student-Newman-Keuls test $p=0.005-0.04$). Additionally, the total
510 dendritic branch lengths in the MS group were shorter than those in the
511 control group (**Fig. 6C**; unpaired Student's t-test, $t(58)=2.01$, $p=0.049$). These
512 results indicate a reduced complexity of dendritic arborization in cortical
513 neurons following MS.

514 The comparison of dendritic spine densities between MS and control
515 groups is illustrated in **Fig. 6D** and **E**. A significantly lower density of basal
516 spines was observed in the MS compared to control groups (**Fig. 6E**, left;
517 unpaired Student's t-test, $t(62)=2.42$, $p=0.019$). Further analysis revealed that

518 the density of mushroom-shaped spines was lower in the MS compared to the
519 control groups (two-way ANOVA, $F(1,186)=3.18$, $p=0.076$; post hoc Student-
520 Newman-Keuls test $p=0.043$), while no significant differences were found
521 between the groups for stubby- and thin-shaped spine densities (post hoc
522 Student-Newman-Keuls test $p=0.94$ for stubby-shaped spines and $p=0.32$ for
523 thin-shaped spines). Similarly, the density of apical dendritic spines in the MS
524 group was significantly lower than that in the control group (**Fig. 6E**, right;
525 unpaired Student's t-test, $t(64)=2.23$, $p=0.03$). Further analysis showed that
526 the densities of mushroom- and thin-shaped spines in the MS group were
527 significantly lower than those in the control group (two-way ANOVA,
528 $F(1,192)=8.72$, $p=0.004$; post hoc Student-Newman-Keuls test $p=0.003$ for
529 mushroom-shaped spines and $p=0.01$ for thin-shaped spines), whereas the
530 stubby-shaped spine densities were comparable between the two groups
531 (post hoc Student-Newman-Keuls test $p=0.66$). Thus, MS induces segment-
532 and type-specific effects on spine protrusion in cortical neurons of adult rats.

533 **Effects of enriched acoustic exposure on MS-induced cortical changes**

534 Early acoustic inputs are crucial for the structural and functional
535 development of cortical neurons (Zhang et al., 2001; Zhou and Merzenich,
536 2008; Zhu et al., 2014; Ouda et al., 2016; Pysanenko et al., 2018; Svobodova
537 Burianova and Syka, 2020). To investigate if early sound exposure can
538 reverse MS-induced cortical changes, a group of MS rats was housed in an
539 EAE during their 3-h daily MS between PND2 and 20, referred to as MS
540 paired with EAE rats (i.e., MS+EAE rats). Serum corticosterone levels in the
541 MS+EAE group were measured on PND21, while sound-azimuth
542 discrimination performance, cortical azimuth tuning, spine density of cortical

543 neurons, and molecular expression were assessed on PND56. These results
544 were then compared with those of the age-matched MS and control groups
545 (**Fig. 7**).

546 As shown in **Fig. 8**, corticosterone levels measured on PND21 were
547 significantly higher in the MS+EAE group compared to the control group (one-
548 way ANOVA, $F(2,33)=19.61$, $p<0.001$; post hoc Student-Newman-Keuls test
549 $p=0.004$), although the values were lower than those observed in the MS
550 group (post hoc Student-Newman-Keuls test $p=0.004$).

551 During the sound-azimuth discrimination task, the MS+EAE group took an
552 average of 6.5 ± 0.8 d and 11.0 ± 1.4 d to achieve 50% and 70% accuracy,
553 respectively. These times were both shorter than those of the MS group (**Fig.**
554 **9A**; one-way ANOVA, $F(2,21)=6.54$, $p=0.006$, post hoc Student-Newman-
555 Keuls test $p=0.027$ for 50% cut-off; one-way ANOVA, $F(2,21)=16.82$, $p<0.001$,
556 post hoc Student-Newman-Keuls test $p<0.001$ for 70% cut-off) but
557 comparable to the control group (post hoc Student-Newman-Keuls test $p=0.34$
558 for 50% cut-off and $p=0.42$ for 70% cut-off).

559 For cortical recording, the distribution of ARs for azimuth-selective curves
560 of cortical neurons in the MS+EAE group shifted significantly to the left
561 compared to the MS group (**Fig. 9B**; Kruskal-Wallis one-way ANOVA,
562 $p<0.0001$; post hoc Dunn's test $p<0.01$), and was now comparable to that of
563 the control group (post hoc Dunn's test $p>0.05$). As expected, the average AR
564 for the MS+EAE group was significantly smaller than that for the MS group
565 (**Fig. 9C**; one-way ANOVA, $F(2,22)=7.94$, $p=0.003$; post hoc Student-
566 Newman-Keuls test $p=0.018$). Thus, the value for the MS+EAE group was

567 effectively not different from that for the control group (post hoc Student-
568 Newman-Keuls test $p=0.20$). Additionally, the distribution of slopes for
569 azimuth-selective curves of cortical neurons in the MS+EAE group shifted
570 slightly to the right compared to the MS group (**Fig. 9D**; Kruskal-Wallis one-
571 way ANOVA, $p<0.0001$; post hoc Dunn's test $p>0.05$), again being not
572 different from the control group (post hoc Dunn's test $p>0.05$). The average
573 slope for the MS+EAE group was also slightly higher than that for the MS
574 group (**Fig. 9E**; one-way ANOVA, $F(2,22)=7.52$, $p=0.003$; post hoc Student-
575 Newman-Keuls test, $p=0.35$), aligning more closely with the control group
576 (post hoc Student-Newman-Keuls test, $p=0.012$).

577 The comparison of dendritic spine densities of cortical neurons revealed
578 that an EAE significantly impacts spine morphology and density in rats
579 exposed to MS. The spine densities of both basal and apical dendrites in the
580 MS+EAE group were significantly higher than those in the MS group (**Fig. 9F**;
581 one-way ANOVA, $F(2,89)=6.00$, $p=0.004$, post hoc Student-Newman-Keuls
582 test $p=0.003$ for basal dendrites and $F(2,92)=4.23$, $p=0.018$, post hoc Student-
583 Newman-Keuls test $p=0.028$ for apical dendrites) and comparable to those in
584 the control group (post hoc Student-Newman-Keuls test $p=0.16$ for basal
585 dendrites and $p=0.76$ for apical dendrites). Additionally, the densities of
586 mushroom-shaped spines in both basal and apical dendrites in the MS+EAE
587 group were significantly higher than those in the MS group (two-way ANOVA,
588 $F(2,267)=5.53$, $p=0.004$, post hoc Student-Newman-Keuls test $p<0.001$ for
589 basal dendrites and $F(2,276)=7.05$, $p=0.001$, post hoc Student-Newman-
590 Keuls test $p<0.001$ for apical dendrites), and aligned more closely with values
591 of the control group (post hoc Student-Newman-Keuls test $p<0.001$ for basal

592 dendrites and $p=0.11$ for apical dendrites). No significant differences in the
593 stubby- and thin-shaped spines were observed between the MS+EAE and MS
594 groups (all post hoc Student-Newman-Keuls test $p>0.49$).

595 These data indicate that exposure to an EAE during the stress period
596 broadly prevents the MS-induced alterations in sound-azimuth discrimination
597 performance, cortical azimuth tuning, and spine density of cortical neurons in
598 adult rats.

599 **Epigenetic regulation of cortical brain-derived neurotrophic factor** 600 **(BDNF)**

601 BDNF plays a crucial role in dendritic spine development and structural
602 plasticity of cortical neurons (Li et al., 2012; Lu et al., 2013; Ramnauth et al.,
603 2022; Wang et al., 2022; Zhang et al., 2023). To begin documenting the
604 molecular alterations accompanying MS-induced cortical changes and their
605 potential restoration to normal values by an EAE, we quantified cortical BDNF
606 expression using quantitative immunoblotting. Results revealed that BDNF
607 level in the MS group was significantly lower than that for the control group
608 (**Fig. 9G**, left panel; one-way ANOVA, $F(2,24)=3.7$, $p=0.04$; post hoc Student-
609 Newman-Keuls test $p=0.035$). In contrast, BDNF expression in the MS+EAE
610 group was not significantly different from that in the control group (post hoc
611 Student-Newman-Keuls test $p=0.082$).

612 Given the known epigenetic regulation of BDNF, we further investigated
613 cortical expression of histone H3 lysine 9 dimethylation (H3K9me2), a
614 modified histone associated with gene silencing, including the repression of
615 BDNF gene transcription (Padeken et al., 2022; Zhao et al., 2022). As shown

616 in the right panel of **Fig. 9G**, H3K9me2 level in the MS group was significantly
617 higher than that in the control group (one-way ANOVA, $F(2,21)=5.32$,
618 $p=0.014$; post hoc Student-Newman-Keuls test $p=0.02$). In contrast, H3K9me2
619 level in the MS+EAE group was significantly lower than that in the MS group
620 (post hoc Student-Newman-Keuls test $p=0.016$) and comparable to that in the
621 control group (post hoc Student-Newman-Keuls test $p=0.61$).

622 These data suggest that MS leads to decreased cortical BDNF
623 expression, potentially through H3K9me2-mediated epigenetic regulation. In
624 contrast, pairing MS with an EAE appears to substantially prevent these MS-
625 induced molecular changes.

626

627 **Discussion**

628 In this study, we established an ELS model by separating the rat pups
629 from their mother for 3 h daily from PND2 to 20. Consistent with earlier studies
630 (Hsu et al., 2003; Koe et al., 2016; Cui et al., 2020; Wang et al., 2020), MS led
631 to lower body weights, increased anxiety-like behaviors, and heightened
632 stress responses, confirming that this neonatal MS protocol successfully
633 induced ELS. We found that MS-induced ELS significantly reduced
634 performance accuracy in the sound-azimuth discrimination task when tested
635 in adulthood, which coincided with broader azimuth tuning and reductions in
636 the dendritic branching and spine density of neurons within the cortical field
637 A1. Our results therefore demonstrate the profound and enduring effects of
638 MS as an ELS on behavioral and cortical processing of sound azimuth. These
639 findings indicate potential consequences of ELS for speech processing and

640 language comprehension in humans, for example, because of the role of
641 spatial hearing in maintaining speech intelligibility in noisy environments
642 (Hawley et al., 2004; Grothe et al., 2010; Zündorf et al., 2013).

643 Previous studies have shown gender differences in the effects of MS-
644 induced ELS. For example, Talani et al. (2023) reported that male, but not
645 female, mice displayed alterations in hippocampal synaptic transmission and
646 cognitive functions, such as spatial memory and novelty preference, following
647 neonatal MS. Additionally, anxiety-like behaviors were observed exclusively in
648 male mice post-MS (Romeo et al., 2003; Bailoo et al., 2014). While some
649 studies have found contrasting results (Veenema et al., 2007; Tsuda and
650 Ogawa, 2012; Cui et al., 2020), the effects of MS tend to be more pronounced
651 in male animals, likely owing to differing hormonal patterns and
652 neurotransmitter interactions between sexes. Furthermore, recent research
653 has shown that MS similarly affects behavioral discrimination of brief gaps in
654 sound for both male and female gerbils (Ye et al., 2023). Based on these
655 findings, this study focused on male rats to examine the impact of MS-induced
656 ELS on auditory processing. Future studies could explore sex-specific effects
657 of MS on cortical processing of sound azimuth.

658 Earlier studies in cats, ferrets, and macaques have shown that lesions in
659 the auditory cortex lead to significant impairments in sound localization
660 (Jenkins and Merzenich, 1984; Kavanagh and Kelly, 1987; Heffner and
661 Heffner, 1990). Similarly, early noise exposure reduces the sound azimuth
662 selectivity of cortical neurons in rats, resulting in diminished performance in
663 spatial discrimination tasks (Xu et al., 2010; Pan et al., 2011; Guo et al.,
664 2012). Conversely, an EAE enhances azimuth tuning of cortical neurons and

665 improves sound localization abilities of rats (Cai et al., 2009). These findings
666 suggest that the auditory cortex is critical for normal sound localization in
667 mammals. It has been proposed that alterations in cortical response selectivity
668 and reliability may affect the neural encoding of acoustic details, thereby
669 impairing auditory-related behaviors (Zhang et al., 2013; Cheng et al.,
670 2017,2020; Liu et al., 2019; Tang et al., 2022). Thus, post-MS changes in
671 cortical azimuth processing may at least partially explain the decrease in
672 discrimination acuity observed in the MS rats during behavioral tasks. Given
673 that the sound-azimuth discrimination task used in this study involves
674 significant learning and memory components, the impact of MS on learning
675 ability and task performance accuracy warrants further investigation.

676 Early auditory inputs are crucial for the structural and functional
677 maturation of neurons in the auditory cortex (Sanes and Woolley, 2011; Kral
678 2013; Chang and Kanold, 2021). Manipulation of auditory inputs during the
679 critical period of cortical development profoundly alters the tuning properties of
680 these neurons, subsequently influencing auditory perception and behavior
681 (Zhang et al., 2001; Han et al., 2007; Xu et al., 2007; Zhou and Merzenich,
682 2008,2009; Popescu and Polley, 2010; Polley et al., 2013; Pysanenko et al.,
683 2018; Bures et al., 2021; Tang et al., 2022). Dendritic spines, which are small
684 membranous protrusions along neuronal dendrites, serve as the primary sites
685 for excitatory synaptic connections (Harris and Kater, 1994; Nimchinsky et al.,
686 2002; Moyer and Zuo, 2018; Akhgari et al., 2024). Therefore, alterations in the
687 dendritic morphology and spine density of cortical neurons can disrupt
688 auditory inputs, leading to changes in neuronal tuning properties (Ouda et al.,
689 2016; Svobodova Burianova and Syka, 2020; Cheng et al., 2022; Tang et al.,

690 2022). In this study, we hypothesized that MS-induced changes in cortical
691 tuning of sound azimuth are associated with modifications in the dendritic
692 morphology and spine density of neurons. Our findings are consistent with this
693 hypothesis: adult MS rats exhibited significantly lower dendritic complexity and
694 dendritic spine density of cortical neurons compared to the controls, at least in
695 the middle cortical layer where physiological recordings were conducted.
696 These changes in dendritic morphology and spine density likely disrupt
697 auditory inputs during cortical development, leading to altered neuronal tuning
698 and behavioral processing. Importantly, the observed morphological
699 alterations may underlie more general changes in auditory processing rather
700 than being limited to spatial processing. Our ongoing research is investigating
701 the post-MS effects on spectral tuning of cortical neurons and frequency
702 discrimination performance to explore this possibility.

703 We further determined whether an EAE could renormalize disrupted
704 dendritic spine development and degraded cortical azimuth tuning caused by
705 MS, thereby restoring behavioral performance. Our results revealed significant
706 changes in dendritic spine density within the cortex of MS+EAE rats,
707 approaching control levels. Furthermore, cortical tuning and behavioral
708 performance in these rats also became nearly indistinguishable from those of
709 the controls. Thus, pairing MS with an EAE generally protects against the
710 changes in cortical spine density observed in adult MS rats, leading to the
711 recovery of cortical azimuth tuning and behavioral outcomes. Since EAE
712 exposure only partially mitigates the elevated corticosterone levels induced by
713 MS, it is conceivable that the beneficial effects of EAE on MS were primarily
714 attributed to its impact on cortical development rather than through a reduction

715 in stress itself. These findings suggest that enriched sensory exposure can
716 serve as an effective strategy to counteract the effects of ELS on sensory
717 function.

718 The molecular mechanisms through which ELS affects the dendritic
719 structure of cortical neurons remain incompletely understood. Previous
720 studies revealed that ELS impacts synaptic structure and connections within
721 cognitive and limbic systems through the epigenetic regulation of BDNF gene
722 expression, since BDNF is crucial for dendrite and spine development
723 (Tenkumo et al., 2020; Jiang et al., 2021; Sun et al., 2021). In addition,
724 epigenetic mechanisms, such as DNA methylation, have been shown to
725 modulate the plasticity of auditory cortex in mice (Schwartz et al., 2020). We
726 thus examined cortical expression of BDNF and its key epigenetic regulator,
727 H3K9me2, in rats exposed to MS. Our findings show that MS significantly
728 downregulated BDNF while upregulating H3K9me2, suggesting that ELS may
729 influence the dendritic structure and spines of cortical neurons through the
730 epigenetic modulation of BDNF gene expression by H3K9me2, thereby
731 influencing the structural and functional changes in neurons within the
732 auditory cortex. These results confirm that this epigenetic regulatory
733 mechanism extends to the sensory cortex, where it appears to play a critical
734 role in mediating the effects of ELS on neuronal structure and function.
735 Interestingly, for rats in the MS+EAE group, cortical levels of BDNF and
736 H3K9me2 were similar to their respective levels in the control group. This
737 finding indicates that exposure to an EAE during MS can potentially prevent
738 ELS-induced changes in neuronal structure and function via a similar
739 regulatory mechanism. It should be noted that methylation pathways, such as

740 those yielding histone H3 lysine 4 trimethylation (H3K4me3) or histone H3
741 lysine 9 trimethylation (H3K9me3), may also influence BDNF gene
742 expression, potentially counteracting or coordinating the effects of H3K9me2
743 (Gupta et al., 2010; Snigdha et al., 2016; Ell et al., 2024). The antagonistic
744 interaction between histone modifications and their impacts on BDNF could
745 represent a dynamic regulatory response to ELS. Therefore, further research
746 is needed to elucidate the detailed molecular mechanisms and explore the
747 roles of additional potential signaling pathways, particularly those involving
748 H3K4me3 and H3K9me3, in the effects of MS-induced ELS on auditory
749 processing.

750 One remaining question is the origin of the cortical changes observed
751 after MS. Here we demonstrated an MS-induced degradation in sound
752 azimuth tuning of cortical neurons. The distinct changes in response
753 characteristics recorded at the cortical level suggest that at least some of
754 these effects may stem from intrinsic cortical remodeling following MS. This
755 idea is further supported by evidence of altered cortical BDNF expression and
756 its epigenetic regulation, as well as changes in the dendritic branching and
757 spine density of cortical neurons, in rats exposed to MS. Additionally, our ABR
758 recordings suggest that MS has little impact on hearing thresholds and neural
759 conduction velocities within the auditory brainstem. However, we cannot
760 exclude the possibility that the observed post-MS changes are partially due to
761 feed-forward responses reflecting altered subcortical processing. Indeed,
762 recent studies on temporal responses of gerbils to sound gaps have reported
763 impairments within the auditory pathway, including the auditory cortex,
764 brainstem, and periphery, following MS (Ye et al., 2023). Therefore, the

765 effects of MS-induced ELS on sound azimuth processing in the subcortical
766 pathway, particularly in the auditory thalamus and inferior colliculus, clearly
767 warrant further investigation.

768

JNeurosci Accepted Manuscript

769 **References**

770 Akhgari A, Michel TM, Vafae MS (2024) Dendritic spines and their role in the
771 pathogenesis of neurodevelopmental and neurological disorders. *Rev*
772 *Neurosci* 35:489-502.

773

774 Alberini CM, Travaglia A (2017) Infantile Amnesia: A Critical Period of
775 Learning to Learn and Remember. *J Neurosci* 37:5783-5795.

776

777 Alves J, de Sá Couto-Pereira N, de Lima RMS, Quillfeldt JA, Dalmaz C (2022)
778 Effects of Early Life Adversities upon Memory Processes and Cognition in
779 Rodent Models. *Neuroscience* 497:282-307.

780

781 Bailoo JD, Jordan RL, Garza XJ, Tyler AN (2014) Brief and long periods of
782 maternal separation affect maternal behavior and offspring behavioral
783 development in C57BL/6 mice. *Dev Psychobiol* 56:674-685.

784

785 Banqueri M, Gutiérrez-Menéndez A, Méndez M, Conejo NM, Arias JL (2021)
786 Early life stress due to repeated maternal separation alters the working
787 memory acquisition brain functional network. *Stress* 24:87-95.

788

789 Barkat TR, Polley DB, Hensch TK (2011) A critical period for auditory
790 thalamocortical connectivity. *Nat Neurosci* 14:1189-1194.

791

792 Bures Z, Popelar J, Syka J (2017) The effect of noise exposure during the
793 developmental period on the function of the auditory system. *Hear Res* 352:1-
794 11.

795

796 Bures Z, Pysanenko K, Syka J (2021) The influence of developmental noise
797 exposure on the temporal processing of acoustical signals in the auditory
798 cortex of rats. *Hear Res* 409:108306.

799

800 Cai R, Guo F, Zhang J, Xu J, Cui Y, Sun X (2009) Environmental enrichment
801 improves behavioral performance and auditory spatial representation of
802 primary auditory cortical neurons in rat. *Neurobiol Learn Mem* 91:366-376.

803

804 Cao X, Huang S, Cao J, Chen T, Zhu P, Zhu R, Su P, Ruan D (2014) The
805 timing of maternal separation affects morris water maze performance and
806 long-term potentiation in male rats. *Dev Psychobiol* 56:1102-1109.

807

808 Chang M, Kanold PO (2021) Development of Auditory Cortex Circuits. *J*
809 *Assoc Res Otolaryngol* 22:237-259.

810

811 Cheng Y, Chen R, Su B, Zhang G, Sun Y, An P, Fang Y, Zhang Y, Shan Y, de
812 Villers-Sidani É, Wang Y, Zhou X (2023) Pairing with Enriched Sound

813 Exposure Restores Auditory Processing Degraded by an Antidepressant. J
814 Neurosci 43:2850-2859.

815

816 Cheng Y, Jia G, Zhang Y, Hao H, Shan Y, Yu L, Sun X, Zheng Q, Kraus N,
817 Merzenich MM, Zhou X (2017) Positive impacts of early auditory training on
818 cortical processing at an older age. Proc Natl Acad Sci U S A 114:6364-6369.

819

820 Cheng Y, Tang B, Zhang G, An P, Sun Y, Gao M, Zhang Y, Shan Y, Zhang J,
821 Liu Q, Lai CSW, de Villers-Sidani É, Wang Y, Zhou X (2022) Degraded
822 cortical temporal processing in the valproic acid-induced rat model of autism.
823 Neuropharmacology 209:109000.

824

825 Cheng Y, Zhang Y, Wang F, Jia G, Zhou J, Shan Y, Sun X, Yu L, Merzenich
826 MM, Recanzone GH, Yang L, Zhou X (2020) Reversal of Age-Related
827 Changes in Cortical Sound-Azimuth Selectivity with Training. Cereb Cortex
828 30:1768-1778.

829

830 Chocyk A, Bobula B, Dudys D, Przyborowska A, Majcher-Maślanka I, Hess G,
831 Wędzony K (2013) Early-life stress affects the structural and functional
832 plasticity of the medial prefrontal cortex in adolescent rats. Eur J Neurosci
833 38:2089-2107.

834

835 Cui Y, Cao K, Lin H, Cui S, Shen C, Wen W, Mo H, Dong Z, Bai S, Yang L,
836 Shi Y, Zhang R (2020) Early-Life Stress Induces Depression-Like Behavior
837 and Synaptic-Plasticity Changes in a Maternal Separation Rat Model: Gender
838 Difference and Metabolomics Study. *Front Pharmacol* 11:102.

839

840 de Villers-Sidani E, Chang EF, Bao S, Merzenich MM (2007) Critical period
841 window for spectral tuning defined in the primary auditory cortex (A1) in the
842 rat. *J Neurosci* 27:180-189.

843

844 Ell MA, Schiele MA, Iovino N, Domschke K (2024) Epigenetics of Fear,
845 Anxiety and Stress - Focus on Histone Modifications. *Curr Neuropharmacol*
846 22:843-865.

847

848 Farrell MR, Holland FH, Shansky RM, Brenhouse HC (2016) Sex-specific
849 effects of early life stress on social interaction and prefrontal cortex dendritic
850 morphology in young rats. *Behav Brain Res* 310:119-125.

851

852 Francis NA, Winkowski DE, Sheikhattar A, Armengol K, Babadi B, Kanold PO
853 (2018) Small Networks Encode Decision-Making in Primary Auditory Cortex.
854 *Neuron* 97:885-897.e6.

855

856 Games KD, Winer JA (1988) Layer V in rat auditory cortex: projections to the
857 inferior colliculus and contralateral cortex. *Hear Res* 34:1-25.

858

859 Grothe B, Pecka M, McAlpine D (2010) Mechanisms of sound localization in
860 mammals. *Physiol Rev* 90:983-1012.

861

862 Guo F, Zhang J, Zhu X, Cai R, Zhou X, Sun X (2012) Auditory discrimination
863 training rescues developmentally degraded directional selectivity and restores
864 mature expression of GABA(A) and AMPA receptor subunits in rat auditory
865 cortex. *Behav Brain Res* 229:301-307.

866

867 Gupta S, Kim SY, Artis S, Molfese DL, Schumacher A, Sweatt JD, Paylor RE,
868 Lubin FD (2010) Histone methylation regulates memory formation. *J Neurosci*
869 30:3589-3599.

870

871 Han YK, Köver H, Insanally MN, Semerdjian JH, Bao S (2007) Early
872 experience impairs perceptual discrimination. *Nat Neurosci* 10:1191-1197.

873

874 Harris KM, Kater SB (1994) Dendritic spines: cellular specializations imparting
875 both stability and flexibility to synaptic function. *Annu Rev Neurosci* 17:341-
876 371.

877

878 Hawley ML, Litovsky RY, Culling JF (2004) The benefit of binaural hearing in
879 a cocktail party: effect of location and type of interferer. *J Acoust Soc Am*
880 115:833-843.

881

882 Heffner HE, Heffner RS (1990) Effect of bilateral auditory cortex lesions on
883 sound localization in Japanese macaques. *J Neurophysiol* 64:915-931.

884

885 Hsu FC, Zhang GJ, Raol YS, Valentino RJ, Coulter DA, Brooks-Kayal AR
886 (2003) Repeated neonatal handling with maternal separation permanently
887 alters hippocampal GABAA receptors and behavioral stress responses. *Proc*
888 *Natl Acad Sci U S A* 100:12213-12218.

889

890 Insanally MN, Köver H, Kim H, Bao S (2009) Feature-dependent sensitive
891 periods in the development of complex sound representation. *J Neurosci*
892 29:5456-5462.

893

894 Jenkins WM, Merzenich MM (1984) Role of cat primary auditory cortex for
895 sound-localization behavior. *J Neurophysiol* 52:819-847.

896

897 Jiang Z, Zhu Z, Zhao M, Wang W, Li H, Liu D, Pan F (2021) H3K9me2
898 regulation of BDNF expression in the hippocampus and medial prefrontal

899 cortex is involved in the depressive-like phenotype induced by maternal
900 separation in male rats. *Psychopharmacology (Berl)* 238:2801-2813.

901

902 Kavanagh GL, Kelly JB (1987) Contribution of auditory cortex to sound
903 localization by the ferret (*Mustela putorius*). *J Neurophysiol* 57:1746-1766.

904

905 Kim EG, Chang W, Shin S, Adhikari AS, Seol GH, Song DY, Min SS (2023)
906 Maternal separation in mice leads to anxiety-like/aggressive behavior and
907 increases immunoreactivity for glutamic acid decarboxylase and parvalbumin
908 in the adolescence ventral hippocampus. *Korean J Physiol Pharmacol* 27:113-
909 125.

910

911 Koe AS, Ashokan A, Mitra R (2016) Short environmental enrichment in
912 adulthood reverses anxiety and basolateral amygdala hypertrophy induced by
913 maternal separation. *Transl Psychiatry* 6:e729.

914

915 Kral A (2013) Auditory critical periods: a review from system's perspective.
916 *Neuroscience* 247:117-133.

917

918 Kraus KS, Carlon B (2012) Neuronal connectivity and interactions between
919 the auditory and limbic systems. Effects of noise and tinnitus. *Hear Res*
920 288:34-46.

921

922 Li Y, Yui D, Luikart BW, McKay RM, Li Y, Rubenstein JL, Parada LF (2012)

923 Conditional ablation of brain-derived neurotrophic factor-TrkB signaling

924 impairs striatal neuron development. Proc Natl Acad Sci U S A 109:15491-

925 15496.

926

927 Liu X, Wei F, Cheng Y, Zhang Y, Jia G, Zhou J, Zhu M, Shan Y, Sun X, Yu L,

928 Merzenich MM, Lurie DI, Zheng Q, Zhou X (2019) Auditory Training Reverses

929 Lead (Pb)-Toxicity-Induced Changes in Sound-Azimuth Selectivity of Cortical

930 Neurons. Cereb Cortex 29:3294-3304.

931

932 Lu B, Nagappan G, Guan X, Nathan PJ, Wren P (2013) BDNF-based synaptic

933 repair as a disease-modifying strategy for neurodegenerative diseases. Nat

934 Rev Neurosci 14:401-416.

935

936 Manzano Nieves G, Bravo M, Baskoylu S, Bath KG (2020) Early life adversity

937 decreases pre-adolescent fear expression by accelerating amygdala PV cell

938 development. Elife 9:e55263.

939

940 Mohedano-Moriano A, Pro-Sistiaga P, Arroyo-Jimenez MM, Artacho-Pérula E,

941 Insausti AM, Marcos P, Cebada-Sánchez S, Martínez-Ruiz J, Muñoz M,

942 Blaizot X, Martinez-Marcos A, Amaral DG, Insausti R (2007) Topographical

943 and laminar distribution of cortical input to the monkey entorhinal cortex. J
944 Anat 211:250-260.

945

946 Monroy E, Hernández-Torres E, Flores G (2010) Maternal separation disrupts
947 dendritic morphology of neurons in prefrontal cortex, hippocampus, and
948 nucleus accumbens in male rat offspring. J Chem Neuroanat 40:93-101.

949

950 Moxon KA, Gerhardt GA, Bickford PC, Austin K, Rose GM, Woodward DJ,
951 Adler LE (1999) Multiple single units and population responses during
952 inhibitory gating of hippocampal auditory response in freely-moving rats. Brain
953 Res 825:75-85.

954

955 Moyer CE, Zuo Y (2018) Cortical dendritic spine development and plasticity:
956 insights from in vivo imaging. Curr Opin Neurobiol 53:76-82.

957

958 Muhammad A, Carroll C, Kolb B (2012) Stress during development alters
959 dendritic morphology in the nucleus accumbens and prefrontal cortex.
960 Neuroscience 216:103-109.

961

962 Nakamura M, Valerio P, Bhumika S, Barkat TR (2020) Sequential
963 Organization of Critical Periods in the Mouse Auditory System. Cell Rep
964 32:108070.

965

966 Nimchinsky EA, Sabatini BL, Svoboda K (2002) Structure and function of
967 dendritic spines. *Annu Rev Physiol* 64:313-353.

968

969 Ohta KI, Suzuki S, Warita K, Kaji T, Kusaka T, Miki T (2017) Prolonged
970 maternal separation attenuates BDNF-ERK signaling correlated with spine
971 formation in the hippocampus during early brain development. *J Neurochem*
972 141:179-194.

973

974 Ouda L, Burianová J, Balogová Z, Lu HP, Syka J (2016) Structural changes in
975 the adult rat auditory system induced by brief postnatal noise exposure. *Brain*
976 *Struct Funct* 221:617-629.

977

978 Padeken J, Methot SP, Gasser SM (2022) Establishment of H3K9-methylated
979 heterochromatin and its functions in tissue differentiation and maintenance.
980 *Nat Rev Mol Cell Biol* 23:623-640.

981

982 Pan Y, Zhang J, Cai R, Zhou X, Sun X (2011) Developmentally degraded
983 directional selectivity of the auditory cortex can be restored by auditory
984 discrimination training in adults. *Behav Brain Res* 225:596-602.

985

986 Paxinos G, Watson C (2005) The rat brain in stereotaxic coordinates. San
987 Diego, CA: Elsevier Academic Press.

988

989 Polley DB, Read HL, Storage DA, Merzenich MM (2007) Multiparametric
990 auditory receptive field organization across five cortical fields in the albino rat.
991 J Neurophysiol 97:3621-3638.

992

993 Polley DB, Steinberg EE, Merzenich MM (2006) Perceptual learning directs
994 auditory cortical map reorganization through top-down influences. J Neurosci
995 26:4970-4982.

996

997 Polley DB, Thompson JH, Guo W (2013) Brief hearing loss disrupts binaural
998 integration during two early critical periods of auditory cortex development.
999 Nat Commun 4:2547.

1000

1001 Popescu MV, Polley DB (2010) Monaural deprivation disrupts development of
1002 binaural selectivity in auditory midbrain and cortex. Neuron 65:718-731.

1003

1004 Pysanenko K, Bureš Z, Lindovský J, Syka J (2018) The Effect of Complex
1005 Acoustic Environment during Early Development on the Responses of
1006 Auditory Cortex Neurons in Rats. Neuroscience 371:221-228.

1007

1008 Ramnauth AD, Maynard KR, Kardian AS, Phan BN, Tippani M, Rajpurohit S,
1009 Hobbs JW, Page SC, Jaffe AE, Martinowich K (2022) Induction of Bdnf from
1010 promoter I following electroconvulsive seizures contributes to structural
1011 plasticity in neurons of the piriform cortex. *Brain Stimul* 15:427-433.

1012

1013 Roger M, Arnault P (1989) Anatomical study of the connections of the primary
1014 auditory area in the rat. *J Comp Neurol* 287:339-356.

1015

1016 Romeo RD, Mueller A, Sisti HM, Ogawa S, McEwen BS, Brake WG (2003)
1017 Anxiety and fear behaviors in adult male and female C57BL/6 mice are
1018 modulated by maternal separation. *Horm Behav* 43:561-567.

1019

1020 Rutkowski RG, Miasnikov AA, Weinberger NM (2003) Characterisation of
1021 multiple physiological fields within the anatomical core of rat auditory cortex.
1022 *Hear Res* 181:116-130.

1023

1024 Rutkowski RG, Weinberger NM (2005) Encoding of learned importance of
1025 sound by magnitude of representational area in primary auditory cortex. *Proc*
1026 *Natl Acad Sci U S A* 102:13664-13669.

1027

1028 Sanes DH, Woolley SM (2011) A behavioral framework to guide research on
1029 central auditory development and plasticity. *Neuron* 72:912-929.

1030

1031 Schwartz BA, Wang W, Bao S (2020) Pharmacological DNA Demethylation
1032 Weakens Inhibitory Synapses in the Auditory Cortex and Re-opens the Critical
1033 Period for Frequency Map Plasticity. *Neuroscience* 440:239-248.

1034

1035 Shin SY, Baek NJ, Han SH, Min SS (2019) Chronic administration of ketamine
1036 ameliorates the anxiety- and aggressive-like behavior in adolescent mice
1037 induced by neonatal maternal separation. *Korean J Physiol Pharmacol* 23:81-
1038 87.

1039

1040 Snigdha S, Prieto GA, Petrosyan A, Loertscher BM, Dieskau AP, Overman
1041 LE, Cotman CW (2016) H3K9me3 Inhibition Improves Memory, Promotes
1042 Spine Formation, and Increases BDNF Levels in the Aged Hippocampus. *J*
1043 *Neurosci* 36:3611-3622.

1044

1045 Sun H, Zhang X, Kong Y, Gou L, Lian B, Wang Y, Jiang L, Li Q, Sun H, Sun L
1046 (2021) Maternal Separation-Induced Histone Acetylation Correlates with
1047 BDNF-Programmed Synaptic Changes in an Animal Model of PTSD with Sex
1048 Differences. *Mol Neurobiol* 58:1738-1754.

1049

1050 Suta D, Rybalko N, Shen DW, Popelar J, Poon PW, Syka J (2015) Frequency
1051 discrimination in rats exposed to noise as juveniles. *Physiol Behav* 144:60-65.

1052

1053 Svobodova Burianova J, Syka J (2020) Postnatal exposure to an acoustically
1054 enriched environment alters the morphology of neurons in the adult rat
1055 auditory system. *Brain Struct Funct* 225:1979-1995.

1056

1057 Talani G, Biggio F, Gorule AA, Licheri V, Saolini E, Colombo D, Sarigu G,
1058 Petrella M, Vedele F, Biggio G, Sanna E (2023) Sex-dependent changes of
1059 hippocampal synaptic plasticity and cognitive performance in C57BL/6J mice
1060 exposed to neonatal repeated maternal separation. *Neuropharmacology*
1061 222:109301.

1062

1063 Tang B, Li K, Cheng Y, Zhang G, An P, Sun Y, Fang Y, Liu H, Shen Y, Zhang
1064 Y, Shan Y, de Villers-Sidani E, Zhou X (2022) Developmental Exposure to
1065 Bisphenol a Degrades Auditory Cortical Processing in Rats. *Neurosci Bull*
1066 38:1292-1302.

1067

1068 Tenkumo C, Ohta KI, Suzuki S, Warita K, Irie K, Teradaya S, Kusaka T,
1069 Kanenishi K, Hata T, Miki T (2020) Repeated maternal separation causes
1070 transient reduction in BDNF expression in the medial prefrontal cortex during
1071 early brain development, affecting inhibitory neuron development. *Heliyon*
1072 6:e04781.

1073

1074 Tsuda MC, Ogawa S (2012) Long-lasting consequences of neonatal maternal
1075 separation on social behaviors in ovariectomized female mice. PLoS One
1076 7:e33028.

1077

1078 Veenema AH, Bredewold R, Neumann ID (2007) Opposite effects of maternal
1079 separation on intermale and maternal aggression in C57BL/6 mice: link to
1080 hypothalamic vasopressin and oxytocin immunoreactivity.
1081 Psychoneuroendocrinology 32:437-450.

1082

1083 Wang CS, Kavalali ET, Monteggia LM (2022) BDNF signaling in context: From
1084 synaptic regulation to psychiatric disorders. Cell 185:62-76.

1085

1086 Wang D, Levine JLS, Avila-Quintero V, Bloch M, Kaffman A (2020)
1087 Systematic review and meta-analysis: effects of maternal separation on
1088 anxiety-like behavior in rodents. Transl Psychiatry 10:174.

1089

1090 Xiao C, Liu Y, Xu J, Gan X, Xiao Z (2018) Septal and Hippocampal Neurons
1091 Contribute to Auditory Relay and Fear Conditioning. Front Cell Neurosci
1092 12:102.

1093

1094 Xu H, Kotak VC, Sanes DH (2007) Conductive hearing loss disrupts synaptic
1095 and spike adaptation in developing auditory cortex. J Neurosci 27:9417-9426.

1096

1097 Xu J, Yu L, Cai R, Zhang J, Sun X (2010) Early continuous white noise
1098 exposure alters auditory spatial sensitivity and expression of GAD65 and
1099 GABAA receptor subunits in rat auditory cortex. *Cereb Cortex* 20:804-812.

1100

1101 Yang J, Harte-Hargrove LC, Siao CJ, Marinic T, Clarke R, Ma Q, Jing D,
1102 Lafrancois JJ, Bath KG, Mark W, Ballon D, Lee FS, Scharfman HE,
1103 Hempstead BL (2014) proBDNF negatively regulates neuronal remodeling,
1104 synaptic transmission, and synaptic plasticity in hippocampus. *Cell Rep* 7:796-
1105 806.

1106

1107 Ye Y, Mattingly MM, Sunthimer MJ, Gay JD, Rosen MJ (2023) Early-Life
1108 Stress Impairs Perception and Neural Encoding of Rapid Signals in the
1109 Auditory Pathway. *J Neurosci* 43:3232-3244.

1110

1111 Zhang K, Wang F, Zhai M, He M, Hu Y, Feng L, Li Y, Yang J, Wu C (2023)
1112 Hyperactive neuronal autophagy depletes BDNF and impairs adult
1113 hippocampal neurogenesis in a corticosterone-induced mouse model of
1114 depression. *Theranostics* 13:1059-1075.

1115

1116 Zhang LI, Bao S, Merzenich MM (2001) Persistent and specific influences of
1117 early acoustic environments on primary auditory cortex. *Nat Neurosci* 4:1123-
1118 1130.

1119

1120 Zhang Y, Zhao Y, Zhu X, Sun X, Zhou X (2013) Refining cortical
1121 representation of sound azimuths by auditory discrimination training. *J*
1122 *Neurosci* 33:9693-9698.

1123

1124 Zhao H, Wang L, Chen L, Zhang J, Sun W, Salvi RJ, Huang YN, Wang M,
1125 Chen L (2018) Temporary conductive hearing loss in early life impairs spatial
1126 memory of rats in adulthood. *Brain Behav* 8:e01004.

1127

1128 Zhao M, Zhu Z, Li H, Wang W, Cheng S, Qin X, Wu H, Liu D, Pan F (2022)
1129 Effects of traumatic stress in adolescence on PTSD-like behaviors, dendrite
1130 development, and H3K9me2/BDNF expression in the amygdala of male rats.
1131 *J Affect Disord* 296:388-399.

1132

1133 Zhou X, Merzenich MM (2008) Enduring effects of early structured noise
1134 exposure on temporal modulation in the primary auditory cortex. *Proc Natl*
1135 *Acad Sci U S A* 105:4423-4428.

1136

1137 Zhou X, Merzenich MM (2009) Developmentally degraded cortical temporal
1138 processing restored by training. *Nat Neurosci* 12:26-28.

1139

1140 Zhu X, Wang F, Hu H, Sun X, Kilgard MP, Merzenich MM, Zhou X (2014)
1141 Environmental acoustic enrichment promotes recovery from developmentally
1142 degraded auditory cortical processing. J Neurosci 34:5406-5415.

1143

1144 Zündorf IC, Lewald J, Karnath HO (2013) Neural correlates of sound
1145 localization in complex acoustic environments. PLoS One 8:e64259.

1146

JNeurosci Accepted Manuscript

1147 **Figure legends**

1148 **Figure 1.** Experimental timelines and procedures for assessing the effects of
1149 maternal separation (MS). The timelines illustrate the procedures performed
1150 on different postnatal days (PNDs) in MS and age-matched control rats. MS
1151 was conducted from PND2 to 20 (orange bar). Body weights were measured
1152 at various intervals between PND2 and 56. Corticosterone (cort) levels and
1153 behavioral assessments, including open field and elevated zero-maze tests,
1154 were conducted on PND21 and 56. Recombinant adeno-associated virus was
1155 bilaterally injected into the primary auditory cortex (A1) on PND28 for
1156 subsequent evaluation of dendritic spines of neurons. On PND56, animals
1157 underwent a sound-azimuth discrimination task, auditory brainstem response
1158 (ABR) recordings, cortical recordings, dendritic spine assessment, and
1159 molecular expression analysis.

1160

1161 **Figure 2.** Signs of stress induced by MS. **A**, Body weight trajectory of MS rats
1162 and age-matched controls on the different PNDs. n=30 on PND2-49 and n=23
1163 on PND56 for the MS group; n=27 on PND2-49 and n=22 on PND56 for the
1164 control group. Error bars represent SEM. +, p<0.01; #, p<0.001. **B**, Individual
1165 body weights on PND35, 42, 49, and 56, showing significant differences
1166 between MS and control groups at each time point. **C**, Representative
1167 movement traces of MS and control groups in the open field test on PND21
1168 (top) and 56 (bottom). **D**, Comparison of distances traveled by MS and control
1169 groups in the open field test in three time ranges (0-5, 5-10, and 10-15 min)
1170 on PND21 (top; n=20 for the MS group and n=19 for the control group) and 56

1171 (bottom; n=30 for the MS group and n=22 for the control group). **E**,
1172 Representative movement traces for MS and control groups in the elevated
1173 zero-maze test on PND21 (top) and 56 (bottom). **F**, Comparison of distances
1174 traveled, open arm entries, and time spent in the open arms by MS and
1175 control groups in the elevated zero-maze test on PND21 (top; n=18 for both
1176 MS and control groups) and 56 (bottom; n=13 for both MS and control
1177 groups). *, p<0.05. **G**, Serum corticosterone levels measured on PND21 (left;
1178 n=12 for both MS and control groups) and 56 (right; n=16 for both MS and
1179 control groups). Values (mean±SEM) are normalized to the age-matched
1180 control group.

1181

1182 **Figure 3.** Effects of MS on sound-azimuth discrimination performance. **A**,
1183 Percent correct on the sound-azimuth discrimination task on different training
1184 days for each of MS (n=8) and control (n=9) rats (left) and average percent
1185 correct for both groups (right). The dashed lines show 50% and 70% of the
1186 maximal scores. Error bars represent SEM. *, p<0.05; +, p<0.01; #, p<0.001.
1187 **B**, Training days to achieve 50% and 70% performance on the task for both
1188 groups. **C**, Percent distribution of azimuth deviations (ADs) on each day, with
1189 positive and negative ADs indicating deviations to the right or left of the target
1190 speaker, respectively, for MS (left) and control (right) groups. **D**, Average ADs
1191 on different training days for both groups.

1192

1193 **Figure 4.** Thresholds and wave latencies of ABRs determined using tone pips
1194 of different frequencies. **A**, Schematic of the experimental setup for ABR

1195 recording. Acoustic stimuli were delivered through a calibrated earphone with
1196 a sound tube positioned inside the external auditory meatus. ABRs were
1197 recorded by placing electrodes (indicated by the arrows) subdermally at the
1198 scalp midline, posterior to the stimulated ear, and on the midline of the back 1-
1199 2 cm posterior to the neck of the animal. **B**, ABR patterns of MS and control
1200 rats in response to tone pips of 10 kHz. The ABR threshold was defined as
1201 the lowest sound intensity capable of eliciting a response pattern
1202 characteristic of that observed at higher intensities (arrow). **C**, ABR thresholds
1203 at different frequencies for MS (n=9) and control (n=10) groups. Error bars
1204 represent SEM. **D**, Latencies of waves I and IV (measured at 70 dB SPL of
1205 acoustic stimuli) for both groups.

1206

1207 **Figure 5.** Degraded cortical azimuth tuning following MS. **A**, Schematic of the
1208 setup for electrophysiological recording in A1. During recording, acoustic
1209 stimuli were delivered from a speaker positioned 34 cm from the head. The
1210 speaker could be placed at any specific azimuth in the frontal auditory space
1211 (0° elevation) using a remote-control system. c or i, contralateral or ipsilateral
1212 relative to the recording site (see also **Materials and Methods**). **B**,
1213 Representative azimuth selectivity curves recorded for control rats,
1214 categorized as azimuth-selective, multipeak, hemifield, or nonselective. **C**,
1215 Percent distribution of cortical azimuth selectivity curves recorded for MS and
1216 control groups. +, p<0.01; #, p<0.001. **D**, Cumulative frequency histograms of
1217 angular ranges (ARs) for MS (n=79) and control (n=74) groups. **E**, Average
1218 ARs for MS (n=9) and control (n=8) groups, using the number of animals as

1219 the sample size. Error bars represent SEM. **F**, Cumulative frequency
1220 histograms of slopes for both groups. **G**, Average slopes for both groups.

1221

1222 **Figure 6.** Dendritic architecture and spine density alterations following MS. **A**,
1223 Representative tracings of dendritic arbors from cortical neurons in MS and
1224 control rats, overlaid with concentric Sholl analysis circles to evaluate dendritic
1225 complexity. Scale bar=100 μm . **B**, Sholl analysis showing the number of
1226 dendritic intersections as a function of distance from the soma in cortical
1227 neurons for MS (n=28) and control (n=26) groups. Error bars represent SEM.
1228 *, p<0.05; +, p<0.01. **C**, Total dendritic length of cortical neurons in MS (n=33)
1229 and control (n=27) groups. **D**, Representative images of dendritic segments
1230 from basal (left) and apical (right) dendrites in MS and control groups. Scale
1231 bar=5 μm . **E**, Quantification of dendritic spine density in basal (left; n=28 for
1232 the MS group and n=36 for the control group) and apical (right; n=36 for the
1233 MS group and n=30 for the control group) dendrites. The inset shows a
1234 schematic representation of spine morphologies.

1235

1236 **Figure 7.** Experimental timelines and procedures for assessing the effects of
1237 an enriched acoustic environment (EAE) on MS-induced changes. Note that
1238 the MS+EAE rats were housed in an EAE during their 3-h daily MS between
1239 PND2 and 20 (gray bar). Corticosterone levels were measured for the
1240 MS+EAE, MS, and control groups on PND21 and sound-azimuth
1241 discrimination performance, cortical recordings, dendritic spine assessment,
1242 and molecular expression analyses were performed on PND56.

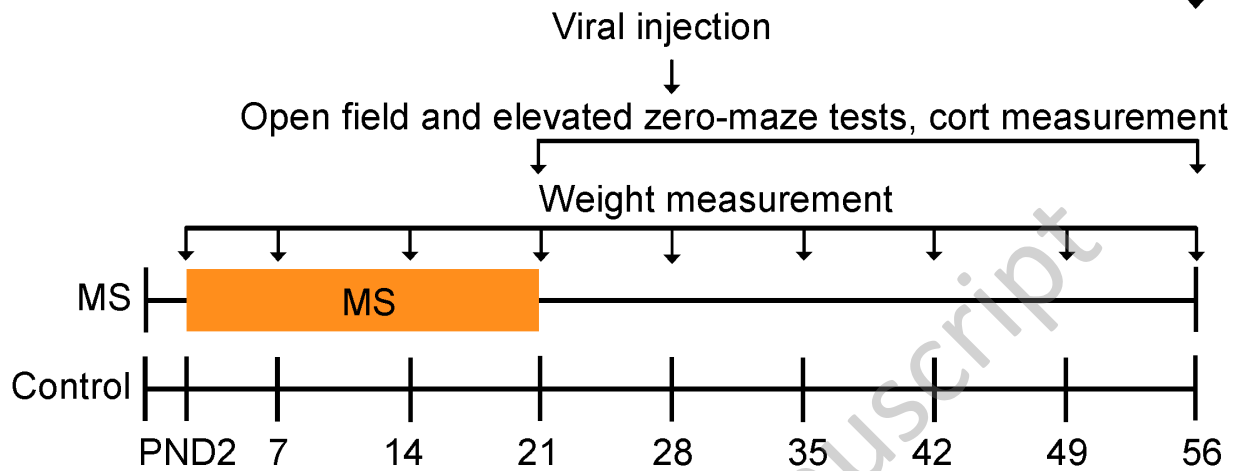
1243

1244 **Figure 8.** Serum corticosterone levels measured on PND21 for the MS+EAE
1245 (n=12), MS, and control groups. Values (mean±SEM) are normalized to the
1246 age-matched control group. +, p<0.01; #, p<0.001.

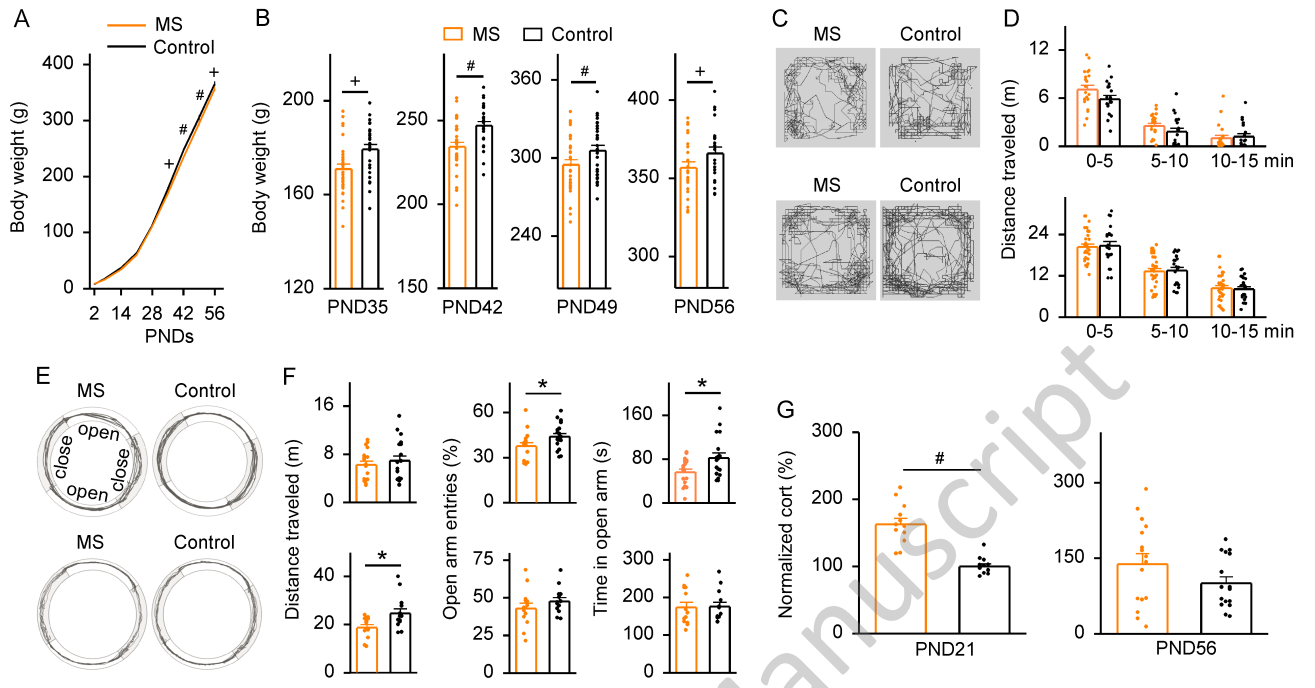
1247

1248 **Figure 9.** Effects of an EAE on MS-induced changes. **A**, Training days to
1249 achieve 50% and 70% performance on the sound-azimuth discrimination task
1250 for the MS+EAE (n=7), MS, and control groups. Error bars represent SEM. *,
1251 p<0.05; +, p<0.01; #, p<0.001. **B**, Cumulative frequency histograms of ARs.
1252 n=71 for the MS+EAE group. **C**, Average AR for each group, using the
1253 number of animals as the sample size. n=8 for the MS+EAE group. **D**,
1254 Cumulative frequency histograms of slopes. **E**, Average slope for each group,
1255 using animals as the sample size. **F**, Quantification of dendritic spine density
1256 in basal (top; n=28 for the MS+EAE group) and apical (bottom; n=29 for the
1257 MS+EAE group) dendrites. The inset shows a schematic representation of
1258 spine morphologies. **G**, Cortical expression levels of brain-derived
1259 neurotrophic factor (BDNF, left panel; n=9 for different groups) and histone H3
1260 lysine 9 dimethylation (H3K9me2, right panel; n=8 for different groups). The
1261 insets show representative Western blots.

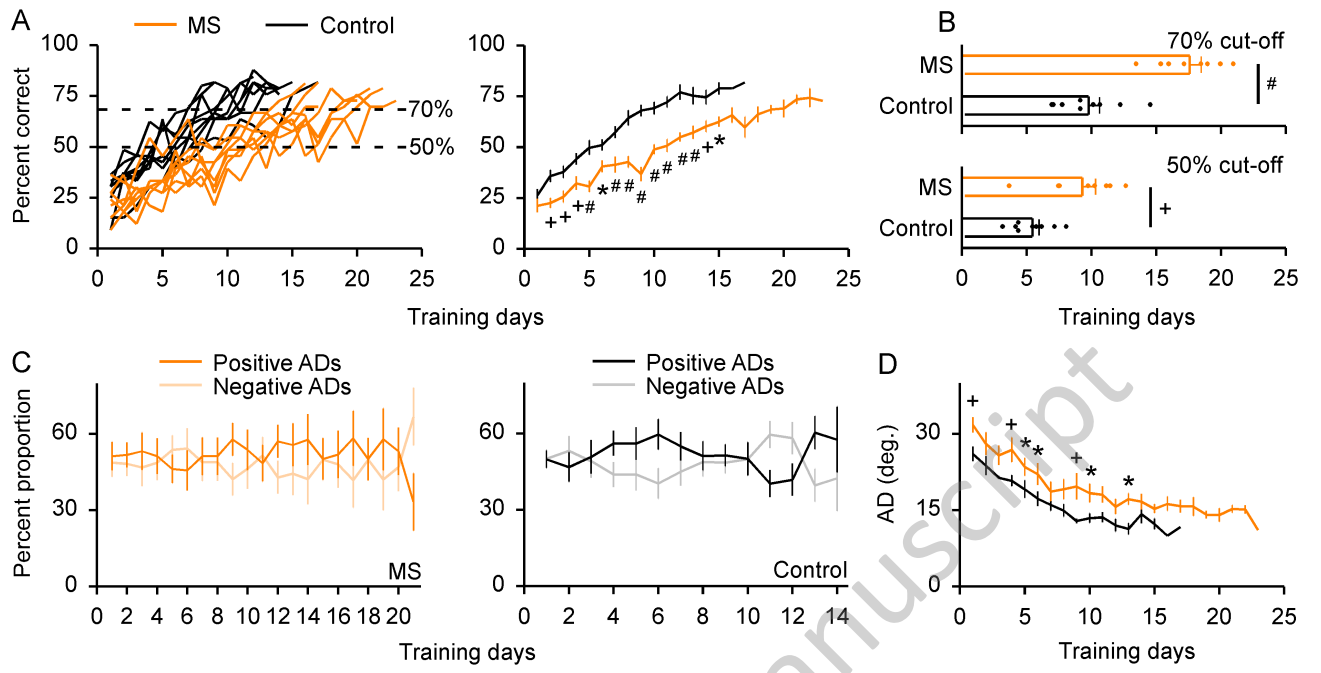
Sound-azimuth discrimination task, ABR and cortical recordings,
dendritic spine assessment, and molecular expression analysis



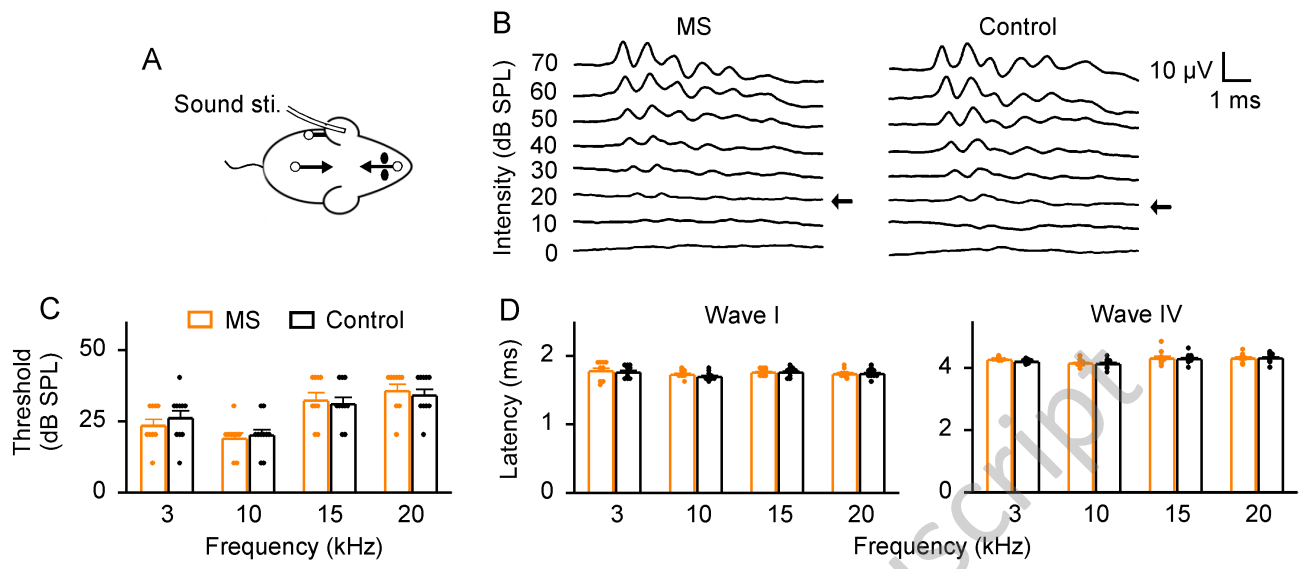
JNeurosci Accepted Manuscript



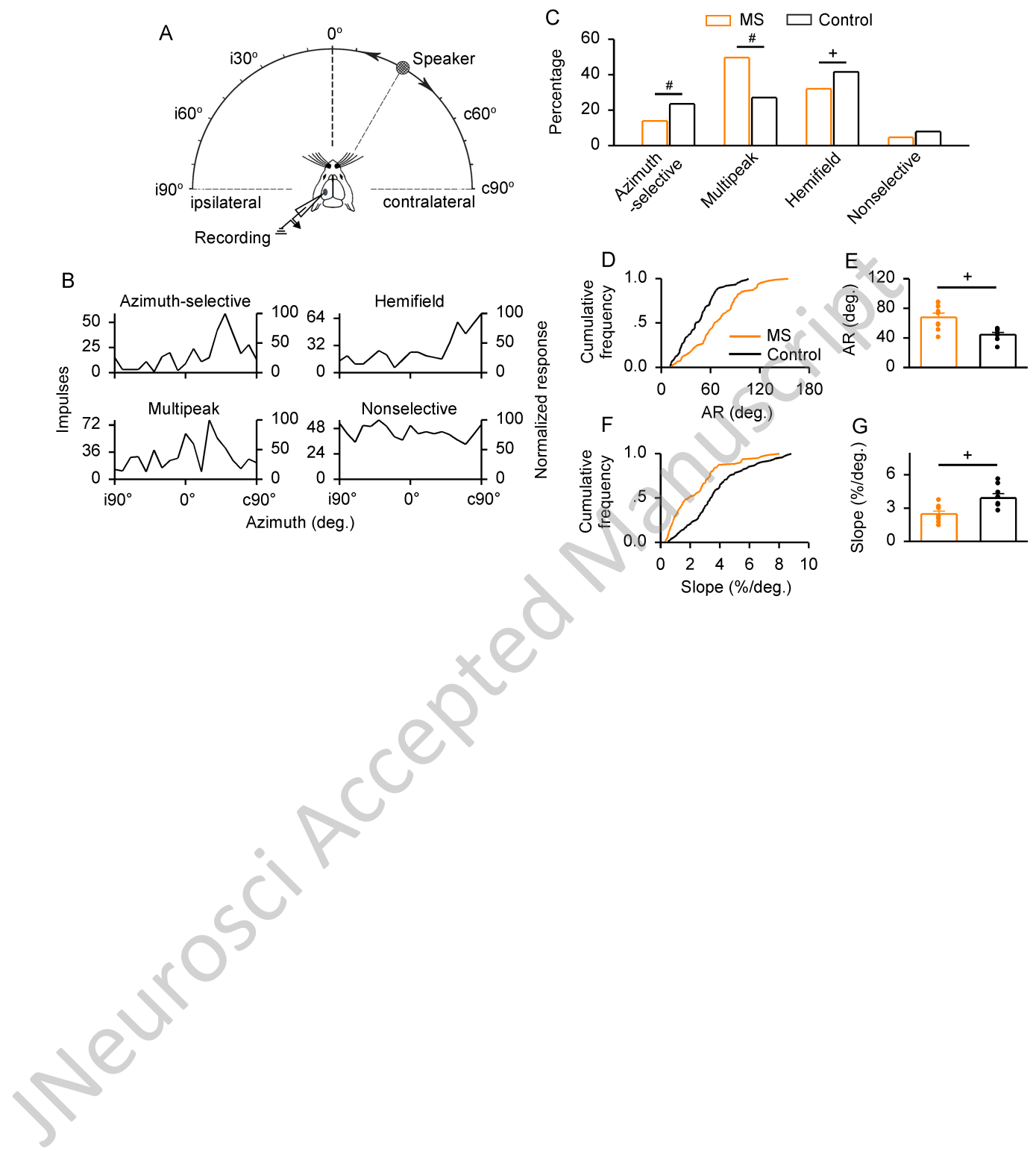
JNeurosci Accepted Manuscript

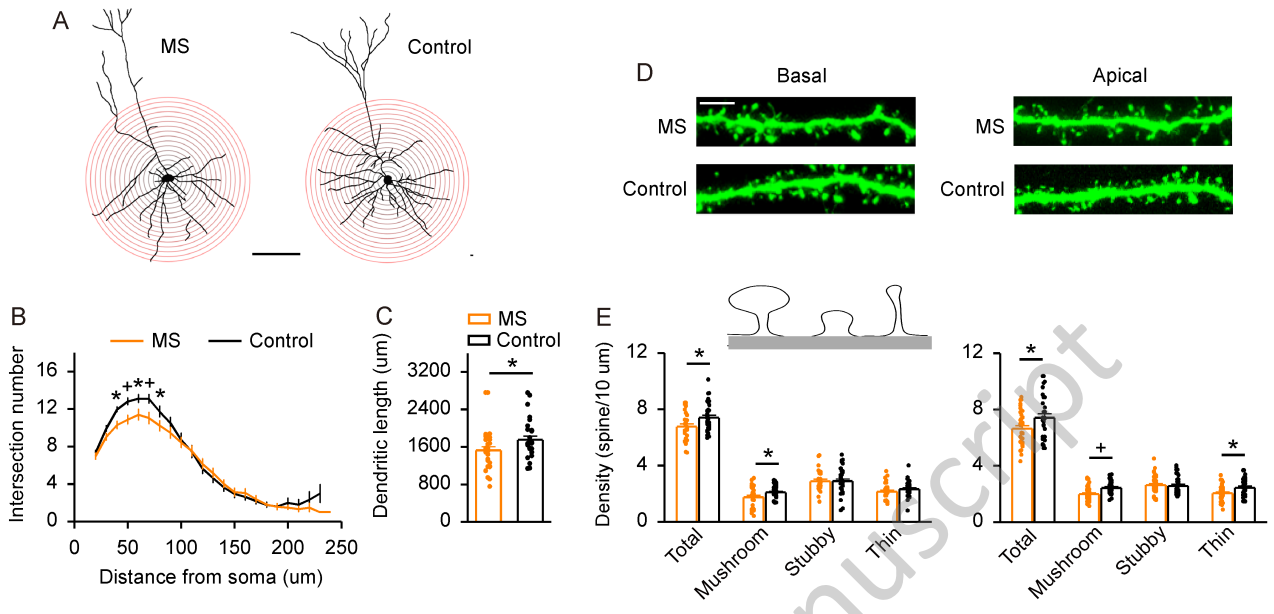


JNeurosci Accepted Manuscript



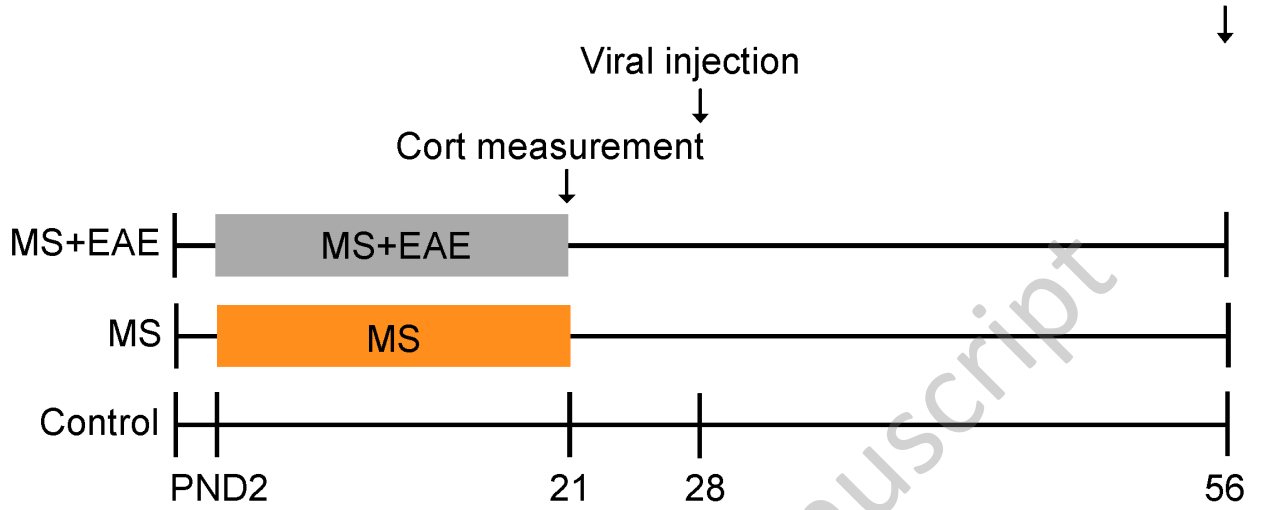
JNeurosci Accepted Manuscript

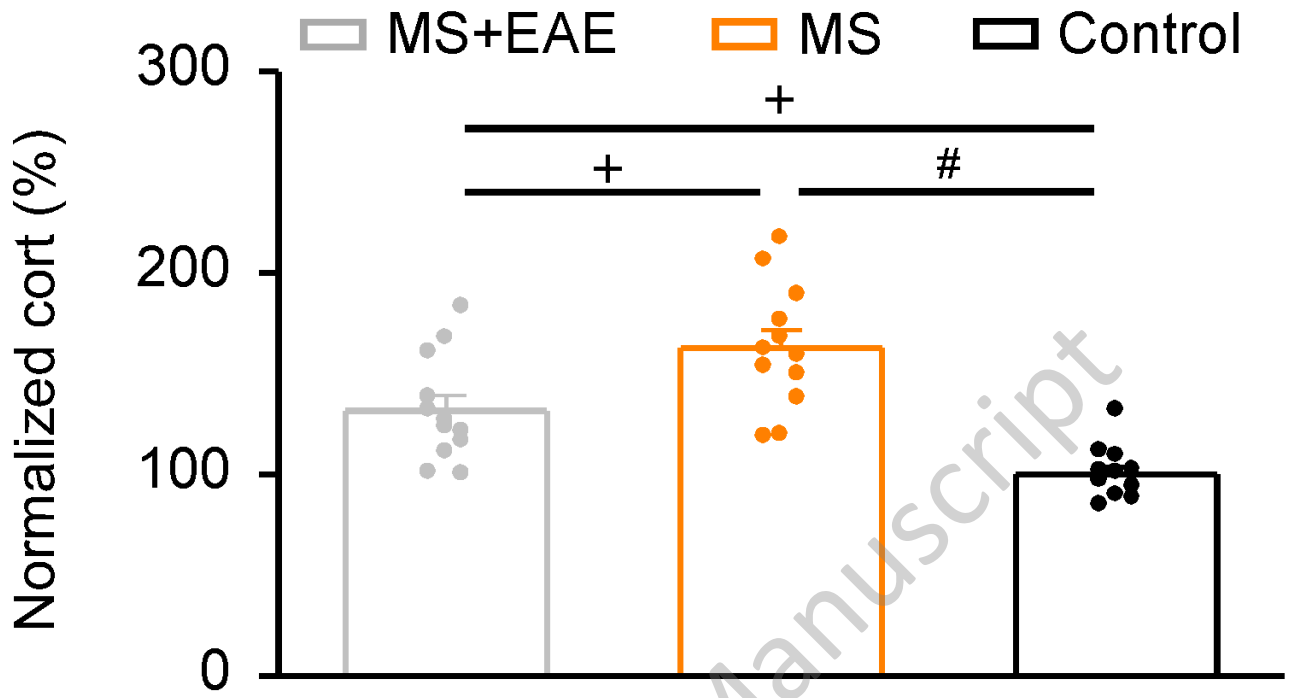




JNeurosci Accepted Manuscript

Sound-azimuth discrimination task, cortical recording, dendritic spine assessment, and molecular expression analysis





JNeurosci Accepted Manuscript

